Tunneling anomaly in superconducting nanograins

Diplomarbeit von

Igor Gazuz

Lehrstuhl für theoretische Festkörperphysik
Sektion Physik
Ludwig-Maximilians-Universität München
Prof. Dr. Jan von Delft

August 2003

Contents

Chapter 1

Introduction

1.1 Motivation

The fascinating phenomenon of superconductivity posed many questions to physisists since its discovery by Kammerlingh Onnes in 1911. A consequent microscopic theory of superconductivity was proposed only in 1957 by Bardeen, Cooper and Shriefer (BCS) [1], as quantum mechanics, originally developed to describe properties of single atoms, has also been successfully applied to macroscipically large condensed matter systems. The BCS theory decribed all observable effects of superconductivity in the bulk like zero resistance, Meissner effect and the gap in the excitation spectrum. The superconductivity turned out to be a purely quantum phenomenon having no counterpart in the classical physics thus being a macroscopic manifestation of the quantum nature of matter.

New fields of physical research, *mesoscopics and nanoscience* (see [2] for an introduction) were opened by new developments in microfabrication techniques during the last several decades, which made it possible to fabricate systems in the submicron range. Such systems "in the middle" between microscopic and macroscopic systems were called *mesoscopic*. *Nanoscience* emphasises small dimensions (1-100 nm).

In the mid-1990s Ralph, Black and Tinkham (RBT) succeeded to perform *single-electron-tunneling spectroscopy* experiments [3] on individual *ultrasmall metallic grains* i. e. small metallic particles on the length scale of several nanomaters The grains were coupled via oxid tunnel barriers to two electrodes and capacitively to a gate to form a single electron transistor with the grain as central island,

and the tunneling current between the grain and the electrodes was measured. From the $I - V$ characteristic of the tunneling current one was able to extract the discrete excitation spectrum of the grains.

The experiments of RBT opend a new frontier in the study of superconductivity, since the excitation spectrum of ultrasmall Al grains with even number of electrons had a distinct spectroscopic gap but an odd grain did not. This was an evidence for the presence of *superconducting pairing correlations* in these grains. Thus new questions could be studied (see [4] for a review), e. g. how does the finite size of the grain affect the superconductivity ? For ultrasmall superconductors the grand-canonical mean-field BCS theory, which was so successful in describing bulk superconductors could not be applied, since the single-particle mean level spacing d was of the same order of magnitude as the bulk superconducting gap Δ. This motivated the development of *canonical theories* of superconductivity.

One interesting feature of the discrete excitation spectra of ultrasmall Al grains measured by RBT was, that the spectroscopic gap was driven to zero by an applied magnetic field. Thus the paramagnetic breakdown of superconducting pairing correlations could be studied in detail. This was done by Braun et. al. [5], who used the *reduced BCS model* to describe the superconducting pairing correlations and solved it via a generalized mean-field Ansatz.

In this thesis we address the following question: how do the pairing correlations affect the single-particle excitation spectrum, in utrasmall metallic grains "*above the paramagnetic limit*", i. e. driven by an applied magnetic field into a paramagnetic state ? We study the *tunneling (or single-particle) density of states* (tuneling DoS) of ultrasmall metallic grains above paramagnetic limit. The tunneling DoS describes the response of a system to adding a single particle to it and thus reflects the correlations inside the system.

We use the reduced BCS model and solve it by means of two *numerical methods* with controllable accuracy. The first method uses the *exact solution* of the reduced BCS model (found by R. Richardson [6]), which expresses the eigenstates and the eigenenergies in terms of certain parameters, which are coupled via a system of algebraical equations. We solve this equations numerically. The second method uses the *density matrix renormalization group* (DMRG) approach for solving the Hamiltonian. The DMRG is a systematical numerical method of studying highly correlated systems, which reduces the Hilbert space of the system by using a small number of basis states that are in particular sense the most probable states that contribute to the ground state (or other targeted states of the system).

First we study the transition to a paramagnetic state. As mentioned, this was already done by Braun et. al. in [5]. But firstly, they used a mean-field approximation and secondly, we need the ground state above paramagnetic limit for calculating the tunneling DoS. We study the crossover between small grains, where the correlations are weak so that this grains behave purely paramagnetically, and large grains, where the correlations are strong so that the BCS theory becomes applicable, which predicts a sharp phase transition between the superconducting and the paramagnetic state.

After considering the transition to a paramagnetic state, we turn to the tunneling density of states. It turns out that in ultrasmall metallic grains above the paramagnetic limit, where the superconducting ground state is destroyed by the applied magnetic field, pair correlations still persist and lead to observable effects, as was predicted by Aleiner and Altshuler (AA) [7], who used diagrammatic techniques and considered the case of *continuous single-electron spectrum* (we call it "continuum limit" in the following). They showed that the tunneling DoS above the paramagnetic limit exhibits an *anomaly*: it has a gap for $0D$ systems (like ultrasmall metallic grains) and a dip for $2D$ systems (like thin films).

The theory of AA was motivated by the experiments of Wu et. al. [8], where an anomaly in the tunneling density of states of disordered superconducting films driven by parallel magnetic field to a paramagnetic state was observed. AA explained this experiments and predicted a new effect in ultrasmall grains.

In this thesis we study the tunneling density of states in ultrasmall superconducting grains using Richardson's exact solution and DMRG. This allows us to study the case of grains with finite number of electrons N and thus with discrete single-electron spectrum. So, we can study deviations from the continuum limit $N \to \infty$ considered by Aleiner and Altshuler.

1.2 Outline

The outline of this thesis is as follows:
In *Chapter 2* the reduced BCS model and methods of solving it are are described. These are the BCS theory, the Richardson's exact solution of the and the DMRG.
Chapter 3 describes the transition of an ultrasmall metallic grain to a paramagnetic state in an applied magnetic field.
In *Chapter 4* the notion of the tunneling density of states is introduced, and the known experimental and analytical results about the tunneling density of states above paramagnetic limit are presented.

In *Chapter 5* our new results for the tunneling DoS of ultrasmall metallic grains with finite number of electrons are presented.
Appendixes A and B contains technical details which are important for understanding exactly how the calculations were done.

Chapter 2

Basics

2.1 The model

We use the discrete *reduced BCS Hamiltonian* with Zeeman coupling to a homogeneous magnetic field [9] :

$$
\begin{aligned}
H_{BCS} &= H_0 + H_{int} && (2.1)\\
H_0 &= \sum_{j,\sigma} (\varepsilon_j - \sigma h)\, c^\dagger_{j\sigma} c_{j\sigma} && (2.2)\\
H_{int} &= -\lambda d \sum_{ij} c^\dagger_{i+} c^\dagger_{i-} c_{j-} c_{j+} && (2.3)
\end{aligned}
$$

Here $c^\dagger_{j\sigma}$ are creators corresponding to the single-electron eigenstates $|\, j\sigma\rangle$ with eigenenergies ε_j. The state $|\, j+\rangle$ is chosen to be the time-reversed to the state $|\, j-\rangle$, where $\sigma = +(-)$ corresponds to the up (down) spin.

The spin projection direction is choosed to be parallel to the magnetic field $\vec{H}$. Thus the Zeeman energy of a spin σ is given by $-\sigma h \equiv \sigma \frac{1}{2} \mu_B g_L H$ with Bohr's magneton μ_B and the Lande factor $g_L = 2$ for electron. The summation in the interacting part H_{int} goes only over levels within the Debye frequency ω_D above and below the Fermi energy ε_F.

The term *"reduced"* in the name of the Hamiltonian referrs to the fact that only time-reversed states participate in the interaction. This Hamiltonian was used by Bardeen, Cooper and Shrieffer in their *BCS theory* of superconductivity [1]. The

interaction described by this Hamiltonian is an effective electron-electron attraction which results from the electron-phonon interaction. The cutoff ω_D appears because ω_D is the typical phonon frequency. The model makes a simplification and uses a constant coupling parameter. This is assumed to capture the most relevant features of the superconductivity phenomena. A good agreement of the calculations made with this model with experiment is the justification of such an assumption.

2.2 BCS theory

The BCS theory describes the superconductivuty in the bulk. The fact that the nubmer of particles is macroscopic allows one to use a *grand-canonical* description:

$$H' = H_{BCS} - \mu N, \tag{2.4}$$

where N is the number of particles. In the grand canocical ensemble the mean value $\langle N \rangle$ rather then N is fixed, which makes the calculations much easier.

In the original work of Bardeen, Cooper and Shrieffer [1] the following Ansatz for the ground state of the superconductor was used:

$$|\,\mathrm{GS}\rangle = \prod_j (u_j + v_j\, c^\dagger_{j+} c^\dagger_{j-})|\,0\rangle \tag{2.5}$$

The parameters u_j and v_j can be interpreted as the probabilities for the level j to be to be empty and to be occupied by a pair of electrons in time reversed states, respectivly. So after performing the tensor product we get a superposition of states with different number of electrons and different amplitudes. BCS used a variational procedure to obtain the optimal u's and v's with the constraint $\langle N \rangle = \mathrm{const}$. They obtained [11]:

$$\left.\begin{matrix} |u_j|^2 \\ |v_j|^2 \end{matrix}\right\} = \frac{1}{2}\left(1 \pm \frac{\varepsilon_j}{E_j}\right), \tag{2.6}$$

where

$$E_j = \sqrt{\Delta^2 + \varepsilon_j^2}, \tag{2.7}$$

and Δ is a solution of the following "*gap equation*":

$$1 = \lambda d \sum_j \frac{1}{\sqrt{\Delta^2 + \varepsilon_j^2}} \tag{2.8}$$

This equation can be solved for bulk systems by replacing the sum over j with the integral over ε. One obtains

$$\frac{\Delta}{d} = \frac{N}{2\sinh(1/\lambda)}, \tag{2.9}$$

where N is the number of interacting levels, which is connected with ω_D via $N/2d = \omega_D$. This means, Δ depends only on ω_D and λ and is a material constant.

Excited states are obtained by breaking the paired states in some of the j's from (2.5). For example, the spin-up electron from a pair at j' goes to a state j'' and the spin-down electron remains in the state j'. One can again make an ansatz similar to (2.5) for such a state:

$$|\,\psi_{\rm exc}\rangle = \left[\prod_{j\neq j',j''} (u_j + v_j\, c^\dagger_{j+} c^\dagger_{j-})\right] c^\dagger_{j'-} c^\dagger_{j''+} |\,0\rangle, \tag{2.10}$$

and then again obtain the u's and v' with a variational method. This way was used in the original paper of Bardeen, Cooper and Shrieffer. There is another way due to Bogoliubov and Valatin ([12, 13]), which uses a *mean-field approximation* of the Hamiltonian H_{BCS} and elucidates the nature of low-energy excited states. One introduces the operators $b_j \equiv c_{j-}c_{j+}$, rewrites the Hamiltonian H_{BCS} in terms of $b_j = \langle b_j\rangle + (b_j - \langle b_j\rangle)$ and then neglects all the terms quadratic in $(b_j - \langle b_j\rangle)$. In this way one reduces the quartic Hamiltonian H_{BCS} to a quadratic one. The latter can be diagonalized by means of a canonical transformation :

$$\begin{aligned} \gamma_{j+} &= u_j\, c_{j+} - v_j\, c^\dagger_{j-} \\ \gamma^\dagger_{j-} &= v^*_j\, c_{j+} + u^*_j\, c^\dagger_{j-} \end{aligned} \tag{2.11}$$

The term "canonical transformation" means here that the commutation relations between the γ-operators remain the same as for the c's. The u's and v's can be choosen in such a way that the Hamiltonian becomes diagonal in $\gamma_{j\sigma}$. This condition leads to exactly the same expressions as for u's and v's from (2.6) The diagonalized Hamiltonian reads:

$$H_{MF} = E_0 + \sum_{j,\sigma} E_j \gamma^\dagger_{j\sigma}\gamma_{j\sigma}, \tag{2.12}$$

where E_j are given by (2.7). Due to the fact that $\gamma_{j\sigma}|\,\mathrm{GS}\rangle = 0$, the operators $\gamma^\dagger_{j\sigma}$ can be interpreted as creations operators of the excitated states. E_j are the corresponding excitation energies and E_0 is the energy of the ground state. The diagonal form of H_{MF} means that the excitations can be created independantly

from each other. They can be interpreted as *quasiparticles*. A general excited state then has the form

$$|\,\psi_{exc}\rangle = \gamma^{\dagger}_{j_1\sigma_1}\ldots\gamma^{\dagger}_{j_n\sigma_n}|\,\mathrm{GS}\rangle \tag{2.13}$$

and the energy

$$E_{exc} = E_1 + \ldots + E_n \tag{2.14}$$

The *condensation energy* of the superconductor is defined as the energy difference between the uncorrelated Fermi sea state and the superconducting ground state:

$$E_{cond} \equiv \langle \mathrm{GS}\,|\,H_{BCS}\,|\,\mathrm{GS}\rangle - \langle \mathrm{FS}\,|\,H_{BCS}\,|\,\mathrm{FS}\rangle \tag{2.15}$$

where $|\,\mathrm{FS}\rangle$ is the uncorrelated Fermi sea state. The calculation with the BCS ground state (2.5) yields:

$$E_{cond} = -\frac{\Delta^2}{2d} \tag{2.16}$$

E_{cond} is proportional to $1/d$, which gives the density of states at the Fermi surface, scaling $\sim$ Vol. Therefore E_{cond} is an extensive quantity. This shows that the superconducting ground state obtained via the ansatz (2.5) is indeed energetically favorable. One can interprete the relation (2.16) as follows: the ground state has $\Delta/2d$ "*Cooper pairs*", each having a binding energy Δ.

2.3 Richardson's exact solution

The reduced BCS model that we use for describing the properties of ultrasmall metallic grains has an exact solution, which was obtained by Richardson ([6], [14]). Before we come to the Richardson's solution, first we describe a property of the Hamiltonian H_{BCS} (2.1), which is called *"blocking effect"*. This means that singly occupied levels *decouple* from the rest of the system (are "blocked") and contribute only with their non-interacting energy. This is a consequense of the fact that $\sum_{i,j} c^{\dagger}_{i+}c^{\dagger}_{i-}c_{j-}c_{j+}$ gives 0 when acting on a state in which level j is singly occupied. Thus if $|\,\psi\rangle$ is an eigenstate with energy E of H_{BCS} with all levels except j interacting, then the state $c^{\dagger}_{j\sigma}\,|\,\psi\rangle$ will be an eigenstate of the H_{BCS} with all levels interacting with energy $E + \varepsilon_j - \sigma h$.

Richardson's exact solution (for a detailed discussion see [9]) yields the eigenstates and eigenenergies for a given set U of *unblocked*, i.e non-singly occupied levels. Every eigenstate corresponds in a one-to-one way to an eigenstate of the non-interacting system, in which the levels from U are either doubly occupied or

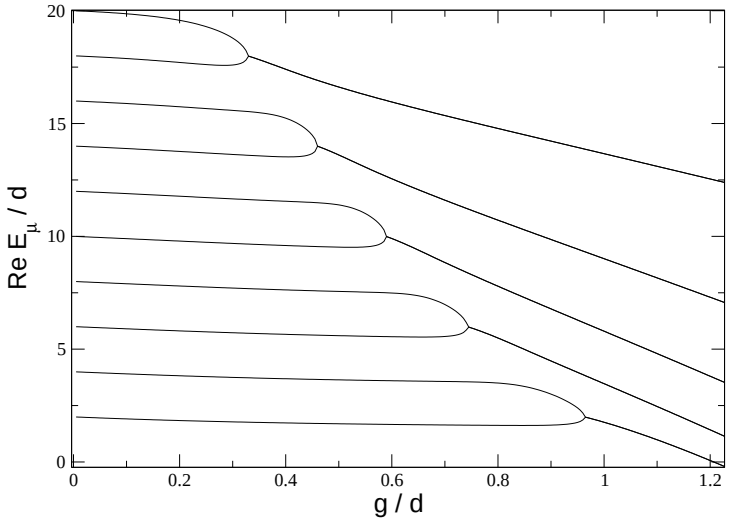

Figure 2.1: The real parts of the energy parameters E_μ from the Richardson's equations (2.17) for $\mu = 1, \ldots, 10$ as a function of coupling parameter. The initial conditions correspond to the ground state.

empty. If there are n pairs of electrons, the eigenstates of the *non-interacting* system are obtained by simply distributing these n pairs among the unblocked levels. If the occupied levels have energies $\varepsilon_1, \ldots, \varepsilon_n$, then the eigenstate has the energy $\sum_{i=1}^{n} 2\,\varepsilon_i$. Now, the corresponding eigenenergy of the *interacting* Hamiltonian can also be written as a sum of certain energy parameters:

$$E = \sum_{i=1}^{n} E_\mu$$

These energy parameters E_μ satisfy the Richardson's equations:

$$1 - \sum_{j}^{U} \frac{g}{2\varepsilon_j - E_\nu} + \sum_{\mu=1(\neq\nu)}^{n} \frac{2g}{E_\mu - E_\nu} = 0, \quad \nu = 1, \ldots, n \tag{2.17}$$

Here the first sum runs over all unblocked levels, and $g = \lambda\, d$ is the coupling constant with the dimension of energy. For $g = 0$ there are no interactions and E_μ must be equal to some noninteracting pair energies : $\forall \mu, E_\mu = 2\,\varepsilon_j$ for

some $j \in U$. When g is increased, E_μ will evolve continuously from their non-interacting values in a way shown in Figure 2.1 for the case of the the ground state (with 10 electron pairs). We see that E_μ (for even N) arrange in pairs whose elements approach each other, and become equal at some value of g. At this point they turn to complex conjugated pairs (in the Figure only the real parts are shown), so that the whole energy remains real.

A general eigenstate can be graphically represented as in Figure 2.2. The circles depict the unblocked levels, where the filled circles depict the levels filled with pairs and the empty ones depict empty levels at $g = 0$. The arrows depict the blocked levels occupied by single electrons. To determine the eigenenergy, we have to solve the Richardson's equations for the unblocked levels with the initial conditions corresponding to the distribution of the filled and unfilled circles and to add the non-interacting energies of the single electrons at the blocked levels to the result.

At the values of g, where some two of the parameters E_μ become equal, Richardson's equations (2.17) become singular. For numerical applications these singularities have to be factored out, which is done in Appendix A for the case of the ground state. For an excited state the energy parameters E_μ behave in quite a complicated way: the pairing between them can change as g is increased (see

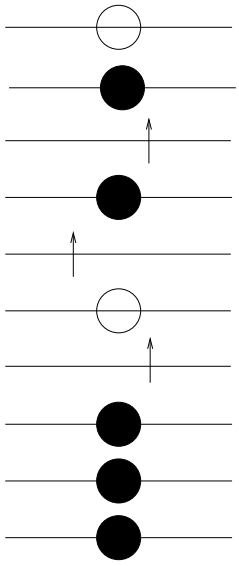

Figure 2.2: A general eigenstate of the reduced BCS Hamiltonian (2.1). The filled circles depict the levels filled with pairs and the empty circles depict the empty levels at $g = 0$. The arrows depict the blocked levels occupied by sinlge electrons.

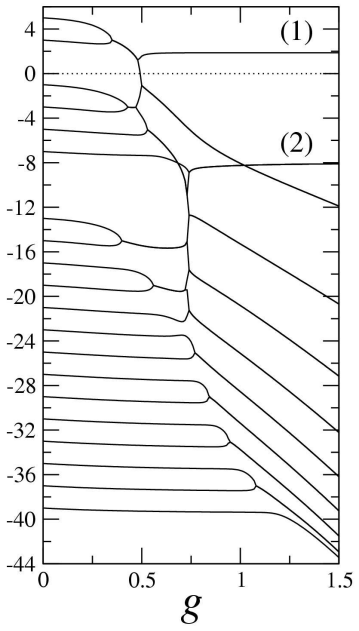

Figure 2.3: This figure from [15] shows the evolution of the Richardson's parameters for an excited state.

Figure 2.3), which means that the algorithm of finding a numerical solution has to be rather sophisticated.

The difficulties of finding the energies of excited states with the exact solution, combined with the difficulty to find with its help the eigenfunctions (which is numerically impossible for $n \gtrsim 8$), caused us to use also another numerical method of solving the reduced BCS Hamiltonian, which is described in the next section.

2.4 Density matrix renormalization group

The density matrix renormalization group (DMRG) is a method invented by S. White to calculate the low-energetical excitations of strongly correlated systems, where the interaction is local (like spin chains) [16]. This method was also succesfully applied to the reduced BCS Hamiltonian by Sierra and Dukelsky [17].

The basic idea of the DMRG method (like in all numerical renormalization strategies) is to find an effective Hamiltonian for a complicated interacting system. This effective Hamiltonian should act on a smaller Hilbert space than the original one

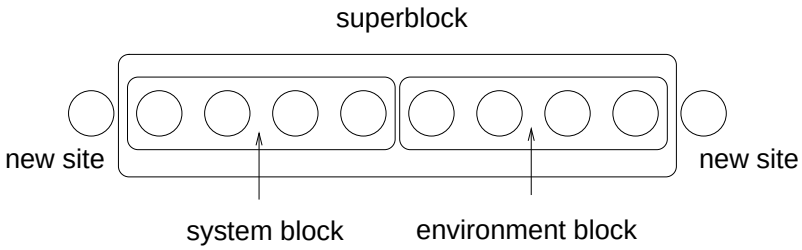

Figure 2.4: DMRG algorithm on a chain

so that it can be solved numerically. At the same time, it should contain the most relevant information about the system.

The idea of using *density matrix* comes from the following observation. Consider an interacting system (*"superblock"*). Let us divide it in two parts , the *"system block"* and the *"environment block"* (see Figure 2.4). If $|\, i\rangle$ and $|\, j\rangle$ are the basis states of the system block and environment block, respectively, a general pure state $|\, \psi\rangle$ of the superblock is given by the sum of the tensor-product states $|\, i\rangle|\, j\rangle$ with some coefficients:

$$|\, \psi\rangle = \sum_{ij} \psi_{ij} |\, i\rangle|\, j\rangle \tag{2.18}$$

We would like now to throw away some states of the system block and to retain only a set m states $|\, u^\alpha\rangle, \alpha = 1, \ldots, m$, namely those which for the fixed value of m would most optimally describe the state $|\, \psi\rangle$ of the superblock. It turns out that if we construct the reduced density matrix of the system block as part of the superblock by tracing out the environment block, and then take its m eigenstates with highest eigenvalues, these states will be the most optimal for describing the superblock. To be precise, this means that the optimal approximation to $|\, \psi\rangle$ is a state $|\, \bar{\psi}\rangle$ of the form

$$|\, \bar{\psi}\rangle = \sum_{\alpha,j} a_{\alpha,j} |\, u^\alpha\rangle|\, j\rangle$$

for which the quantity

$$\mathcal{S} \equiv \Big| |\, \psi\rangle - |\, \bar{\psi}\rangle \Big|^2$$

is minimized by taking for $|\, u^\alpha\rangle$ the m eigenstates whith the largest eigenvalues of the reduced density matrix of the system block $\rho = \mathrm{Tr}_{env}\, (|\, \psi\rangle\langle\psi\, |)$. The corresponding weights $a_{\alpha,j}$ can be constructed from the states $|\, j\rangle$ and the m highest eigenvalues of ρ.

With this idea one can propose several algorithms for finding the ground state and its energy for an interacting system. For a 1-dimensional chain the simplest version of the algorithm ("*infinite system algorithm*") looks like follows:

1. Take a small part of the whole system as the *superblock*. Devide the superblock into the *system block* and the *environment block* (Figure 2.4).

2. *Diagonilize* the superblock Hamiltonian numerically and construct its ground state $|\psi\rangle$.

3. Build the *reduced density matrix* of the system block by tracing out the environment block and find its m eigenvectors with the largest eigenvalues. They will build the *reduced basis* of the system block. Perform the same procedure for the environment block tracing out the system block and obtain the reduced basis of the environment block. The reduced basis of the superblock having $m \times m$ vectors can be obtained by constructing tensor products of the vectors from the reduced bases of the system block and the environment blocks.

4. *Transform* the Hamiltonian of the superblock to the reduced basis from step 3.

5. *Add* a new site to the system block and environment block to form the *new superblock*.

6. *Repeat* with step 2.

The algorithm proposed by Sierra and Dukelsky to find the ground state of the reduced BCS Hamiltonian follows the philosophy of the infinite system algorithm but acts in the momentum space. This means that instead of breaking the superblock into two pieces in the real space, one devides the single-particle levels of the superblock into two parts, one of them spanning the system block and the other spanning the environment block. A general state $|\psi\rangle$ of the superblock can then be represented in the form (2.18) where the states $|i\rangle$ belong to the system subspace and the states $|j\rangle$ belong to the environment subspace. This representation allows one to apply the infinite system algorithm descibed above with the difference, that instead of adding new sites, new single-particle levels are added to the system block and the environment block.

Appendix B contains the details of algorithm of Sierra and Dukelsky for calculating the ground state of the reduced BCS Hamiltonian as well as its modification for the ground state in magnetic field and some of excited states entering into the expression for the tunneling density of states, which is the quantity we are interested in this thesis.

Chapter 3

Transition to a paramagnetic state

In this chapter we shall search for the ground state of an utrasmall superconducting metallic grain in a magnetic field. Without magnetic field the total spin is zero. We will see that the total spin increases with the applied magnetic field.

If a sufficiently large magnetic field is applied to a bulk superconductor, it causes a transition to a normal state. Below the transition point the field can only penetrate the superconductor up to a small surface layer of thickness Λ. This is due to the surface currents generated when the field is turned on, that screen the magnetic field in the interior of the superconductor. So a bulk superconductor behaves as a perfect diamagnet until the magnetic field reaches a certain critical value and destroys the superconductivity.

Ultrasmall metallic grains as those from experiments of Ralph, Black and Tinkham have radii $r \lesssim 5\,\mathrm{nm}$ and are smaller than the penetration depth of the magnetic field $\Lambda \sim 50\,\mathrm{nm}$. Thus all their electrons interact with the magnetic field. This interaction gives rise to two types of magnetic effects: Pauli paramagnetism, associated with Zeeman splitting of electron orbitals and Landau diamagnetism, associated with the orbital motion of electrons. The latter effect can be shown to be negligible in ultrasmall metallic grains [10]. This is why only the Zeeman term is contained in our model Hamiltonian (2.1).

In section 3.1 normal paramagnets are considered. Their spin increases linearly with the magnetic field. In section 3.2 bulk superconductors are considered, where the BCS theory [1] can be applied. Here a first order *phase transition* from superconducting to a purely paramagnetic state occurs. In section 3.3 we turn

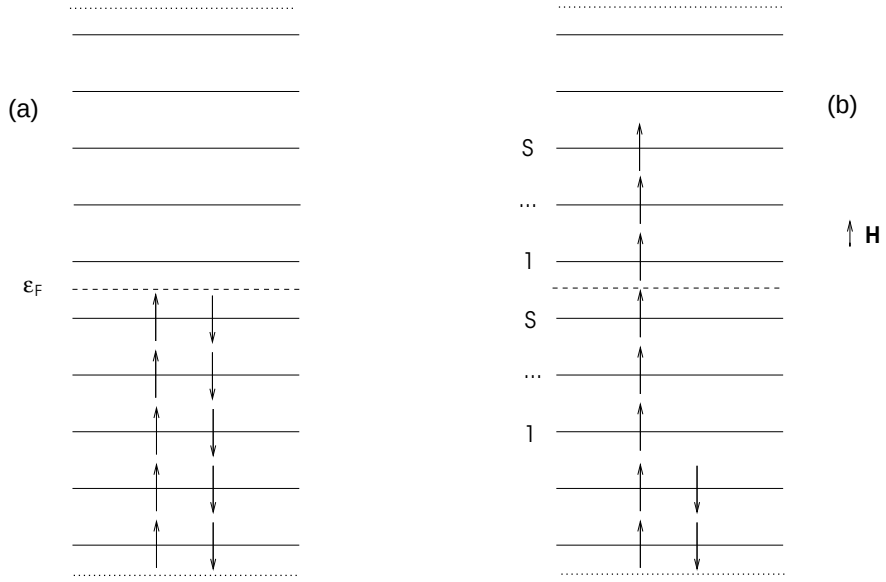

Figure 3.1: Ground state of a normal grain without magnetic field (a) and with magnetic field $\vec{H}$ (b). The electrons gain energy if they choose their spin parallel to $\vec{H}$ but have to pay kinetic energy due to the Pauli principle. For a given $\vec{H}$, the spin S can be determined by maximizing the energy gain.

to ultrasmall superconducting grains. Here by varying the electron number N and coupling constant λ we can reach both the weak coupling regime ($\Delta/d \ll 1$), where the behaviour is similar to that of normal paramagnets and the strong coupling regime ($\Delta/d \gg 1$), where the BCS theory can be applied.

3.1 Normal paramagnets

In this Section we consider a normal paramagnet, having no interaction, so that every energy eigenstate of the grain is a direct product of some single-particle eigenstates. In absence of magnetic field the ground state is obtained by filling up the single-particle energy levels with pairs of electrons with opposite spins up to the Fermi energy ε_F (see Figure 3.1(a)).

A magnetic field $\vec{H}$ breaks the two-fold degeneracy of energy levels due to the Zeeman interaction $-\sigma h$. Thus the levels occupied by single electrons with spins parallel to $\vec{H}$ decrease their energy by h while the doubly occupied levels do not change their energy. So it can be favorable for some electrons to flip their spin

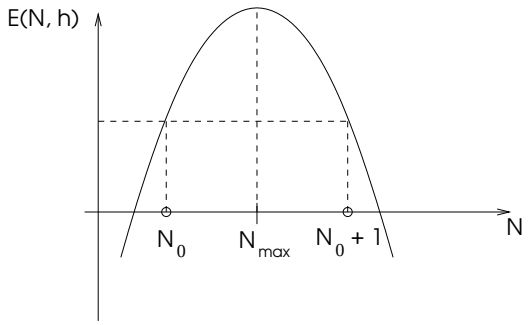

Figure 3.2: Energy gain vs. number of flipped spins N

and (due to Pauli principle) to jump to unoccupied (higher) energy levels if the gain in magnetic energy becomes greater then the loss in kinetic energy. Let the number of flipped spins be S. Then S will also be the *spin* of the system (in units of $\hbar$). It is clear that for every given S the lowest possible state is that where the flipped electrons were immediately below ε_F before changing their spin.

If there are S singly occupied levels below ε_F and S singly occupied levels above ε_F with spins parallel to $\vec{H}$ (see Figure 3.1(b)), and we choose ε_F as the zero of the energy scale, the kinetic energy of the electrons at the singly ocupied levels will be equal to zero because of their symmetrical distribution with respect to ε_F. Before flipping these electrons were at the S doubly occupied levels immediately below ε_F and they had the energy $-\sum_{i=0}^{S-1} 2\,(\frac{1}{2}+i)\cdot d = -S^2\,d$. Therefore the loss in the kinetic energy is $S^2 d$. On the other side, the magnetic energy of $2S$ spins parallel to magnetic field is $-2Sh$, and before flipping the magnetic energy was equal to zero, i.e the gain in the magnetic energy is $2Sh$ and we can obtain S for given h by maximizing the energy gain

$$E(S,h) = 2Sh - S^2\,d$$

For given h, this is a function of a discrete variable S. We can find it's maximum by considering the corresponding function of a continuous variable. Its graph is a parabola which is symmetric about its maximum point

$$S_{max}(h) = h/d. \tag{3.1}$$

The shape of the parabola is only determined by the factor near S^2, so it does not depend on h. For $h = 0$ the most favorable state is $S = 0$ and when h is increased, the transition from S_0 to $S_0 + 1$ occurs if $E(S)$ becomes equal for $S = S_0$ and $S = S_0 + 1$, i.e if $S_{max}(h)$ lies in the middle between S_0 and $S_0 + 1$ (see Figure 3.2).

Thus the transition from S to $S+1$ occurs at the points

$$h = (S + 1/2)\, d, \quad S = 0, 1, 2 \ldots \tag{3.2}$$

The corresponding spin increases also by 1 (in units of $\hbar$). The first jump occurs at $h = \frac{d}{2}$ and the next jumps are separated from each other by d.

For a bulk system, where S can be considered as a continuous variable, $1/d$ corresponds to the density of states $g(\varepsilon_F)$ at the Fermi surface and the spin will go linearly with h:

$$S = S_{max}(h) = h\, g(\varepsilon_F). \tag{3.3}$$

So the magnetization $M = \mu_B \cdot S$ is given by $\mu_B h\, g(\varepsilon_F) = \mu_B^2 H\, g(\varepsilon_F)$ and the susceptibility is $\chi = \partial M/\partial H = \mu_B^2\, g(\varepsilon_F)$, which is the well known *Pauli paramagnetic susceptibility* [18].

The difference between the ground state energy in magnetic field h and without magnetic field $E_{GS}(h) - E_{GS}(0) = E(N_{max}(h), h)$ is:

$$E_{GS}(h) - E_{GS}(0) = -\frac{h^2}{d} \tag{3.4}$$

3.2 Bulk superconductors

In the bulk limit the BCS theory can be applied. We assume that at some critical field h_c the system changes it's spin by a macroscopically large amount and becomes purely paramagnetic, with no pairing correlations anymore (it will be justified in the next paragraph). This happens if the ground state energy difference of the pure paramagnet $E_{GS}(h) - E_{GS}(0)$ (see eq. (3.4)) becomes smaller than the bulk condensation energy of the superconductor, which is equal to $-\Delta^2/2d$ (see equation (2.16)). So we have

$$\frac{h_c^2}{d} = \frac{\Delta^2}{2d},$$

which yields :

$$h_c = \frac{\Delta}{\sqrt{2}}. \tag{3.5}$$

With (3.3) the spin increase is

$$S_c = \frac{\Delta}{\sqrt{2}d} \overset{(2.9)}{=} \frac{N}{2\sqrt{2}\sinh(1/\lambda)} \tag{3.6}$$

The assumption that in the paramagnetic state no pair correlations persist anymore, is justified by the following argument: the excitations in the pair correlated state are obtained by breaking cooper pairs and pairwise creating of quasiparticles (see Section 2.2). The lowest such a state is obtained by breaking one Cooper pair and creating two quasiparticles wich costs the energy $2\Delta - 2h$, and this becomes favorable at $h = \Delta$, which is larger than h_c.

So we see, that in the strong coupling limit a *phase transition* from superconducting to a purely paramagnetic state occurs. The transition is of the first order because of the discontinuity in the magnetization as order parameter at the critical value of the magnetic field h_c.

3.3 Ultrasmall superconducting grains

In this section we consider the transition to a paramagnetic state for ultrasmall superconducting grains. If a magnetic field is applied to the grain, then, to construct Richardson's solution (see chapter 2, section 2.3) we have to start by considering the states corresponding to the non-interacting case described in section 3.1. This means, we have some singly occupied, blocked levels lying immediately below and above ε_F. We shall consider a grain with even number of electrons N (if N were odd, we had one blocked electron in the ground state without magnetic field, and for the remaining even number of electrons the physics would not change).

Let us call N_F the number of levels which correspond to the non-interacting levels filled with pairs, and N_B the number of blocked levels (see Figure 3.3). Then $N_B + 2N_F = N$. The blocked electrons contribute only with their kinetic energy and additional magnetic energy $-h$ per level. The remaining $2N_F$ electrons are scattered between the $2N_F$ unblocked levels due to the pairing interaction (2.3). We call their total energy E_{int}.

In contrast to the non-interacting case, we have no analytical expression for E_{int} and have to find it numerically. The total energy of the grain for a given number of blocked levels, $E(N_B)$ is then given by

$$E(N_B, h) = E_{kin}(N_B) + E_{int}(N_B) - N_B h$$

For given h, the optimal N_B can be found by compairing $E(N_B, h)$ for all possilble $N_B = 0, 2, \ldots, N$ (since by flipping of one spin the number of blocked levels increases by 2). Then $\mu_B N_B$ gives the magnetization of the system. The kinetic energy of N_B blocked electrons $E_{kin}(N_B)$ is equal to ε_F due to their symmetrical

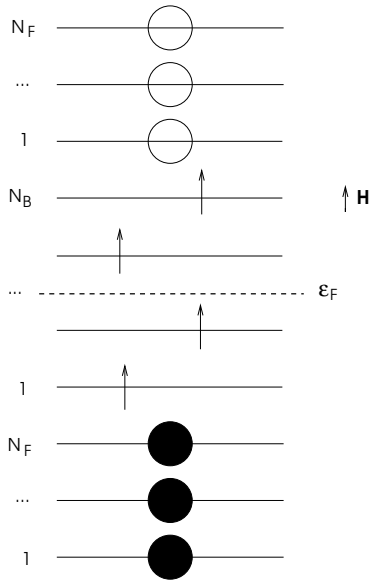

Figure 3.3: Candidates for the ground state of the grain. The N_B levels immediately above and below ε_F are occupied by single electrons with spins parallel to the magnetic field. The remaining $2N_F$ electrons are scattered among the $2N_F$ unblocked levels. The distribution of filled circles corersponds to the initial values of the Richardson's parameters (see Section 2.3).

distribution with respect to ε_F. So it is constant for a given grain and will be droped in the following.

For calculating the energy of the unblocked electrons two methods were used: numerical solving of Richardson's equations and DMRG (see Sections 2.3, 2.4 for introduction and Appendixes A, B for details). Thus we could combine the power of DMRG with the possibility to check the calculations made with its help against the results from Richardson's exact solution in a regime were both methods work.

In Figure 3.4 we show the total energy of the grain $E(N_B, h)$ vs. h for all possible N_B for $N = 20$ and $\lambda = 0.8$. We see that from some critical value of h the state with $N_B = 0$ becomes unfavorable and the spin begins to increase.

In Figure 3.5 the magnetization vs. magnetic field is shown for $N = 20$ and different values of λ. We see that for small λ the behaviour is normal: the first spin flip occurs at $h = d/2$ and the next are separated by d. With increasing λ the value of the first spin jump, S_{first}, increases. After the first flip the spin increases by 1 at each step, just like in the normal regime. But if the state after

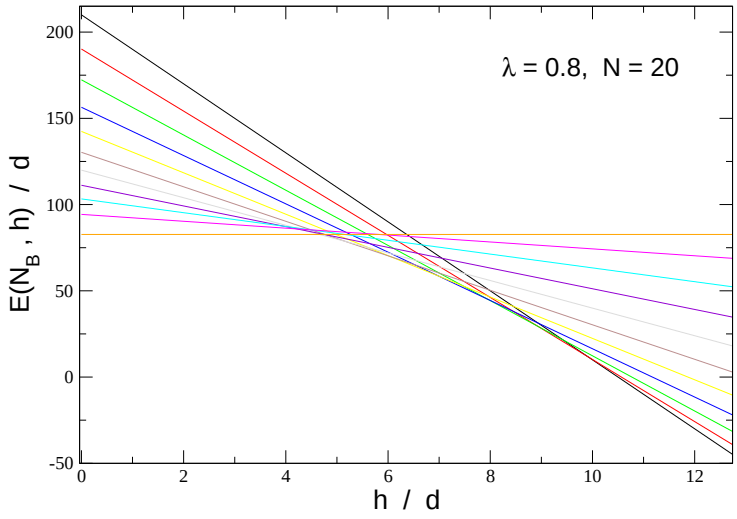

Figure 3.4: Total energy of the grain $E(N_B, h)$ (in units d) for $\lambda = 0.8$, $N = 20$ and different blocking numbers $N_B = 0, 2, \ldots, 20$ vs. magnetic field h (in units of d). The lowest line corresponds to $N_B = 0$, the top line to $N_B = 20$. For some value of h, the superconducting ground state with $N_B = 0$ (and thus zero spin) becomes unfavorable and the spin begins to increase.

the first spin flip would be normal, than the values of the magnetic field at which the subsequent spin flips occur, should coincide with the values of the magnetic field, at which spin flips for the normal grain occur. We see from Figure 3.5 that this is not the case. This is an evidence for the remnants of pairing fluctuations in the paramagnetic state.

In Figure 3.6 we plotted the magnetization vs. magnetic field for fixed λ and different values of N. The behaviour of the magnetization with increasing N is similar to the case of fixed N and increasing λ just discussed. In both cases the value of Δ/d is increased, thus the pairing correlations become stronger and the bulk BCS regime is approached.

To study the *crossover* between the weak coupling and strong coupling regimes by varying Δ/d from being $\ll 1$ to $\gg 1$, we calculate the height of the first spin jump, S_{first}, and the corresponding magnetic field h_{first} for different values of N and λ. Since $\Delta/d = N/(2\sinh(1/\lambda))$ (see (2.9)), we can increase Δ/d both by increasing N at fixed λ and by increasing λ at fixed N.

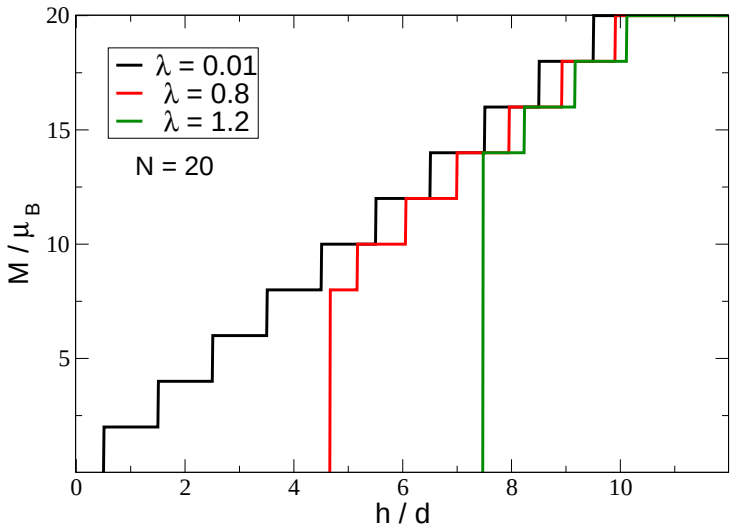

Figure 3.5: Magnetization M (in units of μ_B) vs. magnetic field h (in units of d) for $N = 20$ and different values of λ. With increasing λ the first spin jump, S_{first}, increases.

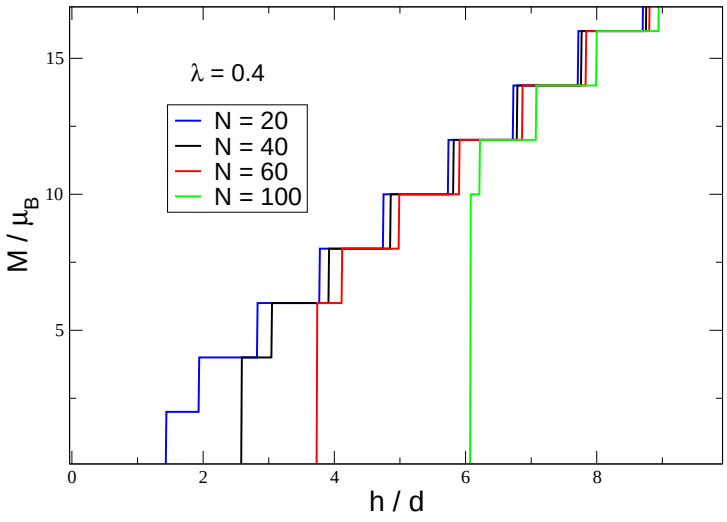

Figure 3.6: Magnetization M (in units of μ_B) vs. magnetic field h (in units of d) for $\lambda = 0.4$ and different values of N. With increasing N the first spin jump, S_{first}, increases

In Figure 3.7 the ratios S_{first}/S_c and h_{first}/h_c vs. N for fixed λ are plotted, where S_c and h_c are the bulk BCS critical values for spin and magnetic field (see eqs. (3.6) and (3.5). With increasing N, h_{first}/h_c converges rather fast to unity from above. The plot of S_{first}/S_c vs. N consists of continuous decreasing parts with jumps between them. This is due to the discrete nature of the variable S_{first}, which in contrast to linearly growing S_c (see (3.6)) does not change along every continuous part (the leftmost continuous part corresponds to $S_{first} = 1$) so that S_{first}/S_c decreases. At the values of N, where S_{first} increases, S_{first}/S_c jumps up and then again decreases continuously with increasing N until the new change of S_first occurs. The oscillations become smaller with increasing N and the S_{first}/S_c converges to unity from below.

So we see, that with increasing N, the S_{first} and h_{first} approach their bulk BCS values S_c and h_c. For small N the deviations from the BCS theory are significant: the ratios S_{first}/S_c and h_{first}/h_c differs from 1 by more than 0.5.

In Figures 3.8, 3.9, S_{first}/S_c and h_{first}/h_c vs. λ for fixed N are shown . The agreement with BCS theory for large λ is much worse then for the case of constant λ and increasing N. This is not surprising, even though for increasing λ and fixed N, Δ/d also increases. For at some value of $\lambda = \lambda_{cr}$, all spins will flip, thus for $\lambda > \lambda_{cr}$ S_{first} will remain constant, while S_c will still increase linearly with λ, since for fixed N equation (3.6) yields

$$S_c \propto 1/\sinh(1/\lambda) \sim \lambda \quad \text{for} \quad \lambda \gtrsim 1 \tag{3.7}$$

The reason for this disagreement the continuum limit, that underlies the BCS theory. Therefore it does not take into account the fact that the number of particles is finite.

The quantity h_{first}, which has a continuius range of values, still increases even when all spins are flipped. It lies below the BCS critical field h_c. It is interesting that for $\lambda > \lambda_{cr}$, h_{first} increases almost linearly with λ.

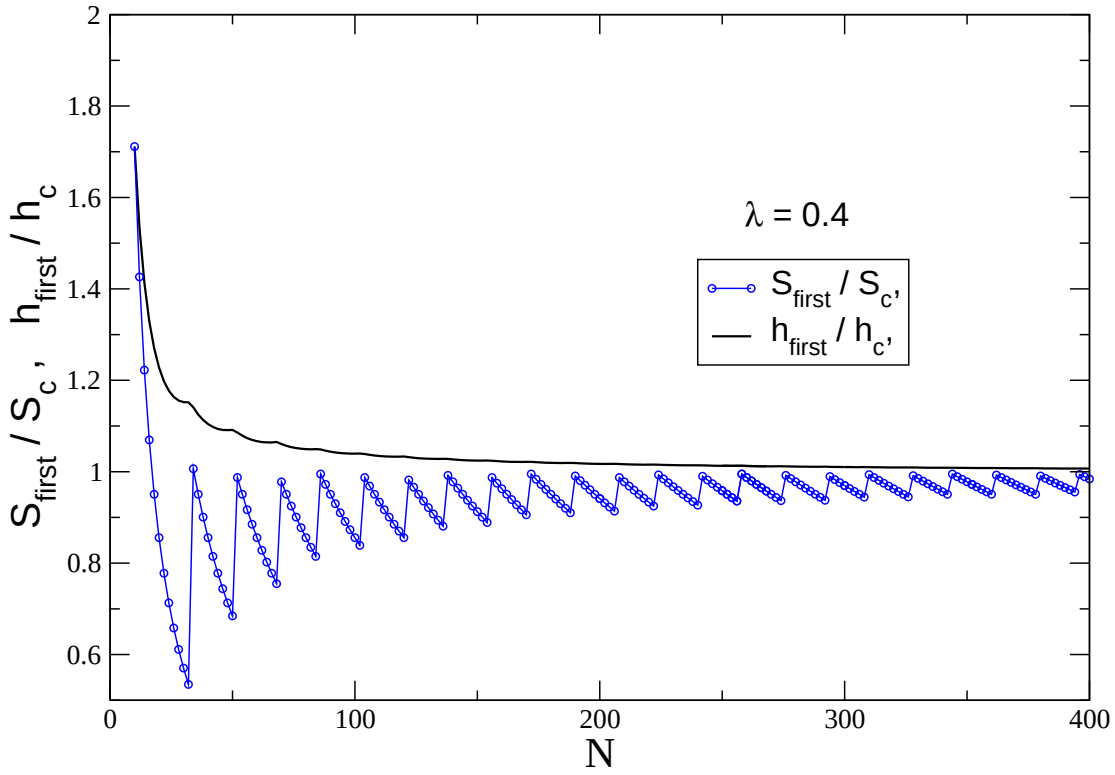

Figure 3.7: S_{first}/S_c and h_{first}/h_c vs. number of electrons N for $\lambda = 0.4$. With increasing N the first spin jump S_{first} and the corresponding magnetic field h_{first} approach their BCS bulk values S_c and h_c (see eqs. (3.6), (3.5)).

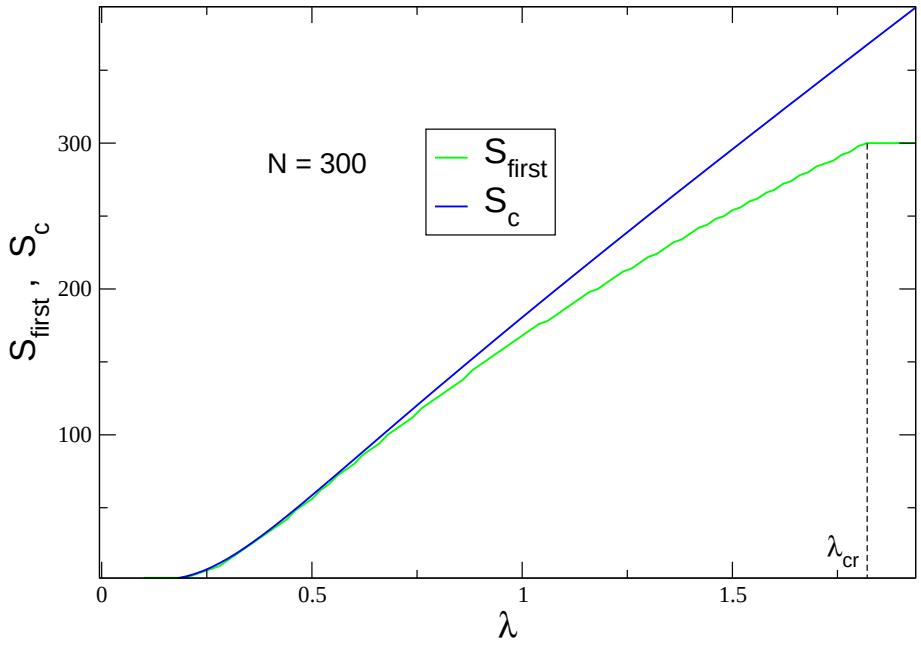

Figure 3.8: S_{first} and S_c (in units of $\hbar$) vs. λ for $N = 300$.

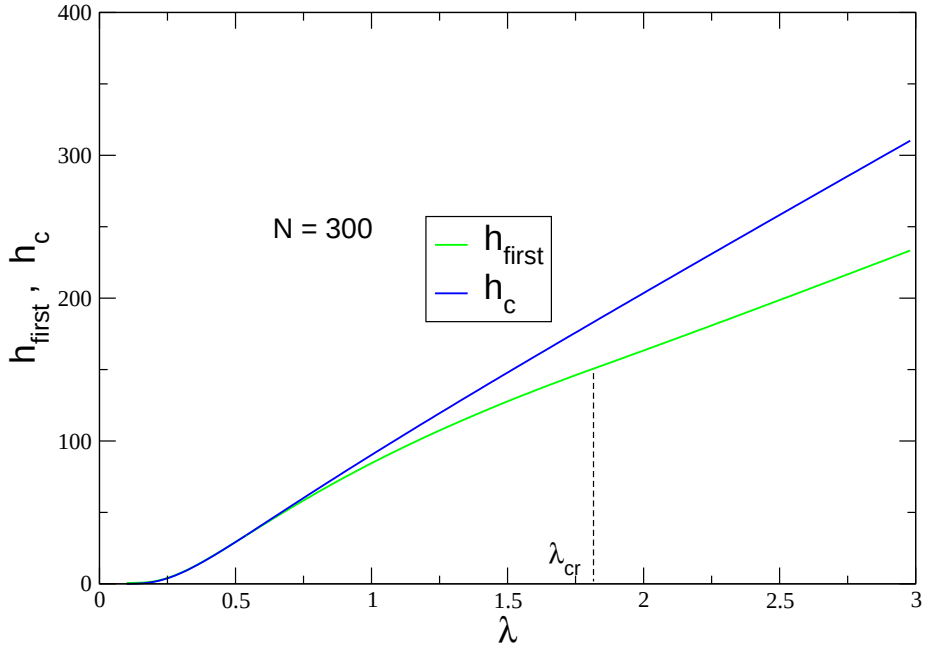

Figure 3.9: h_{first} and h_c (in units of d) vs. λ for $N = 300$.

Chapter 4

Tunneling anomaly above paramagnetic limit: known results

In this chapter we introduce the notion of tunneling (or single-particle) density of states (tunneling DoS). It is a quantity that measures the response of a system to adding a single particle to it. The tunneling DoS can be measured via tunneling experiments with single-electron transistors, where the electrons jump individually from the lead to the sample. The tunneling DoS can be expressed via the Green's function of the sample and therefore it can be calculated using the Feynman diagrammatic technique.

First we shall look at the tunneling DoS of a bulk superconductor. There it turns out that the tunneling density of states is equal to the BCS quasiparticle density of states. Then we present the results of Aleiner and Altshuler [7] for the tunneling DoS of an ultrasmall grain above the paramagnetic limit, i.e for a magnetic field that is large enough to cause a transition from the superconducting to the normal state, as considered in chapter 3. These results were motivated by the experiments of Wu et. al. [8], who made the first direct measurement of the e-e interaction anomaly in a disordered 2D superconductor.

4.1 The tunneling density of states

Consider a model of a tunneling experiment[1] (Figure 4.1). There is a lead on the left side and a sample on the right side of the junction with a tunneling barrier between them. A bias voltage is applied to the tunneling junction that causes a chemical potention difference between the lead and the sample. So the system is in non-equilibrium and a current can flow. The tunneling process can be described by means of the effective *tunneling Hamiltonian*:

$$H_T = \sum_{\mathbf{k},\mathbf{k}'} \left(T_{\mathbf{k}\mathbf{k}'} a^\dagger_{\mathbf{k}} b_{\mathbf{k}'} + T^*_{\mathbf{k}\mathbf{k}'} b^\dagger_{\mathbf{k}'} a_{\mathbf{k}} \right), \tag{4.1}$$

where $a^\dagger$ and $b^\dagger$ are the single-electron creators of the lead and the sample, respectively. The full Hamiltonian is given by the sum

$$H = H_1 + H_2 + H_T, \tag{4.2}$$

where H_1 and H_2 are the Hamiltonians of the lead and the specimen, respectively.

The tunneling current can be expressed as the rate of the change of the number of electrons on the lead. This rate can be found in the Heisenberg picture from

$$I = \dot{Q}_a = i[H, Q_a], \quad Q_a = e \sum_{\mathbf{k}} a^\dagger_{\mathbf{k}} a_{\mathbf{k}}. \tag{4.3}$$

Since both H_1 and H_2 conserve the charge of the lead, only H_T gives a contribution to the current. In order to find the average current we have to find the averge of the operator $\dot{Q}_a$ in the state where the chemical potentials of the both sides of the junction are different. This is a non-equilibrium state and one cannot directly

[1] The discussion in this section follows [19]. See also [20]

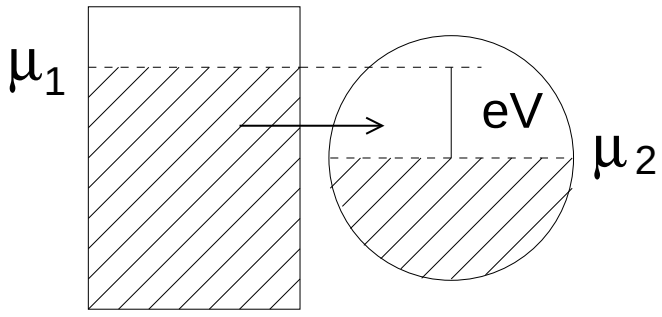

Figure 4.1: A tunneling experiment

apply the usual equilibrium techniques like the linear response theory. But one can use a standard trick which allows us to map the problem on an equivalent equilibrium problem. It consists in making the following gauge transformation:

$$a_{\mathbf{k}} \to a_{\mathbf{k}}, \quad b_{\mathbf{k}'} \to b_{\mathbf{k}'} e^{ieVt} \tag{4.4}$$

This transformation shifts the energies in the sample at eV and therefore it balances the chemical potentials. After this transformation the tunneling Hamiltonian becomes

$$H_T = X e^{ieVt} + X^\dagger e^{-ieVt}, \tag{4.5}$$

where

$$X = \sum_{\mathbf{k},\mathbf{k}'} T_{\mathbf{k}\mathbf{k}'} a^\dagger_{\mathbf{k}} b_{\mathbf{k}'}, \tag{4.6}$$

and the tunneling current is given by

$$I = ie(X e^{ieVt} - X^\dagger e^{-ieVt}). \tag{4.7}$$

So, after the gauge transformation (4.4) we get a time-dependent perturbation acting on an equilibrium state. It means that we can apply the Kubo formula and calculate the current as the linear response of the time-dependent current operator (4.7) to the "external field" (4.5). The bias voltage eV gives the frequency of the "external field".

Now, according to the Kubo formula (see e.g. [20]), the average of the tunneling current operator (4.7) in the lowest order of peturbation theory with the tunneling Hamiltonian (4.5) as perturbation is given by

$$\overline{I(t)} = i \int_{-\infty}^{t} dt' \langle [H_T(t'), I(t)] \rangle \tag{4.8}$$

Consider the susceptibility $\chi(\omega)$,

$$\chi(\omega) = i \int_0^\infty dt \, \langle [X(t), I(0)] \rangle e^{i\omega t}, \tag{4.9}$$

which describes the response of the tunneling current to the external field X (see equation (4.6)). The tunneling current as a function of voltage V is related to $\chi(\omega)$ via

$$I(V) = 2\mathrm{Re}\, \chi(\omega = eV) \tag{4.10}$$

In order to calculate $\chi(\omega)$, first we consider the Matsubara susceptibility

$$\chi_M(i\Omega_n) = \frac{1}{2} \int_{-\beta}^{\beta} d\tau \langle \mathrm{T}_\tau X(\tau) I(0) \rangle e^{i\Omega_n \tau}, \tag{4.11}$$

and then continue it to the real frequencies. Substituting into (4.11) the expressions for I and X from (4.7) and (4.6), we obtain

$$\langle \mathrm{T}_\tau X(\tau) I(0)\rangle = \\ ie \sum_{\mathbf{k_1},\mathbf{k_1'},\mathbf{k_2},\mathbf{k_2'}} T_{\mathbf{k_1 k_1'}} \langle \mathrm{T}_\tau a^\dagger_{\mathbf{k_1}}(\tau) b_{\mathbf{k_1'}}(\tau) \left(T_{\mathbf{k_2 k_2'}} a^\dagger_{\mathbf{k_2}}(0) b_{\mathbf{k_2'}}(0) - T^*_{\mathbf{k_2 k_2'}} a_{\mathbf{k_2}}(0) b^\dagger_{\mathbf{k_2'}}(0)\right)\rangle \tag{4.12}$$

In abscence of superconducting correlations in the lead and the sample the averages $\langle a^\dagger_{\mathbf{k}} a^\dagger_{\mathbf{k'}}\rangle$ and $\langle b_{\mathbf{k}} b_{\mathbf{k'}}\rangle$ are equal to zero. Therefore only the second term in (4.12) gives a non-zero contribution. (This argument also holds if only one of the sides of the junction is non-superconducting, which will be the case in the next section.) So, we get

$$\langle \mathrm{T}_\tau X(\tau) I(0)\rangle = -ie \sum_{\mathbf{k k'}} |T_{\mathbf{k k'}}|^2 G_a(\tau, \mathbf{k}) G_b(-\tau, \mathbf{k'}), \tag{4.13}$$

where $G_a(\tau, \mathbf{k}) = -\langle \mathrm{T}_\tau a_{\mathbf{k}}(\tau) a^\dagger_{\mathbf{k}}(0)\rangle$ and $G_b(\tau, \mathbf{k}) = -\langle \mathrm{T}_\tau b_{\mathbf{k}}(\tau) b^\dagger_{\mathbf{k}}(0)\rangle$ are the Matsubara Green's functions of the lead and the sample, respectively. Writing the Green's functions as Fourier integrals and substituting in (4.11), we obtain

$$\chi_M(i\Omega_n) = -2ieT \sum_{\omega_m} \sum_{\mathbf{k k'}} |T_{\mathbf{k k'}}|^2 G_a(i\omega_m + i\Omega_n, \mathbf{k}) G_b(i\omega_m, \mathbf{k'}), \tag{4.14}$$

where T is the temperature the factor 2 comes from the summation over spin projections.

Now we perform the analytical continuation of the expression (4.14). We use the expresses of the Matsubara Green's function in terms of the spectral function, i. e. the imaginary part of the retarded Green's function (see e.g. [20]):

$$G(i\omega_n, \mathbf{r_1}, \mathbf{r_2}) = \frac{1}{\pi} \int_{-\infty}^{\infty} d\omega \, \frac{\mathrm{Im}\, G^R(\omega, \mathbf{r_1}, \mathbf{r_2})}{\omega - i\omega_n} \tag{4.15}$$

As a result, the Matsubara susceptibility (4.14) becomes

$$\chi_M(i\Omega_n) = -2ieT \sum_{\omega_m} \sum_{\mathbf{k k'}} |T_{\mathbf{k k'}}|^2 \int_{-\infty}^{\infty} \int \frac{d\omega d\omega'}{\pi^2} \frac{\mathrm{Im}\, G^R_a(\omega, \mathbf{k}) \mathrm{Im}\, G^R_b(\omega', \mathbf{k'})}{(i\omega_m + i\Omega_n - \omega)(i\omega_m - \omega')} \tag{4.16}$$

The sum over ω_n can be calculated with the help of the identity (see [19])

$$T \sum_{\omega_m} \frac{1}{(i\omega_m + i\omega_n - \xi_{p+k})(i\omega_m - \xi_p)} = \frac{n_F(\xi_{p+k}) - n_F(\xi_p)}{i\omega_n - \xi_{p+k} + \xi_p} \tag{4.17}$$

It yields

$$\chi_M(i\Omega_n) = -\frac{2ie}{\pi^2} \sum_{\mathbf{k k'}} |T_{\mathbf{k k'}}|^2 \int_{-\infty}^{\infty} d\omega d\omega' \, \mathrm{Im}\, G^R_a(\omega, \mathbf{k}) \mathrm{Im}\, G^R_b(\omega', \mathbf{k'}) \frac{n_F(\omega) - n_F(\omega')}{\omega' - \omega + i\Omega_n} \tag{4.18}$$

The analytical continuation of this expression to real frequencies is obtained by substituting $\omega+i0$ for of $i\Omega_n$. According to (4.10), the real part of the analytically continuated expression yields the tunneling current

$$I(V) = \frac{4e}{\pi}\sum_{\mathbf{kk'}} |T_{\mathbf{kk'}}|^2 \int_{-\infty}^{\infty} d\omega d\omega' \, \delta(\omega'-\omega-eV) \mathrm{Im}\, G_a^R(\omega,\mathbf{k}) \mathrm{Im}\, G_b^R(\omega',\mathbf{k'}) (n_F(\omega)-n_F(\omega')) \tag{4.19}$$

Integrating over ω eliminates the δ-function and finally, we get:

$$I(V) = 4e\sum_{\mathbf{k},\mathbf{k'}} T_{\mathbf{k},\mathbf{k'}}^2 \int_{-\infty}^{\infty} \frac{d\omega}{\pi} \mathrm{Im}\, G_a^R(\mathbf{k},\omega+eV) \mathrm{Im}\, G_a^R(\mathbf{k'},\omega) \left[n_F(\omega) - n_F(\omega+eV)\right], \tag{4.20}$$

where n_F is the Fermi distribution function. If we neglect the $\mathbf{k}$-dependence of the tunneling amplitudes $T_{\mathbf{k},\mathbf{k'}}$ and set $T_{\mathbf{k},\mathbf{k'}} = T_0$, equation (4.20) becomes:

$$I(V) = 4\pi e|T_0|^2 \int_{-\infty}^{\infty} d\omega \nu_a(\omega+eV)\nu_b(\omega) \left[n_F(\omega) - n_F(\omega+eV)\right], \tag{4.21}$$

where

$$\nu_{a(b)}(\omega) \equiv -\frac{1}{\pi}\sum_{\mathbf{k}} \mathrm{Im}\, G_{a(b)}^R(\mathbf{k},\omega) \tag{4.22}$$

is the *tunneling (or single-particle) density of states.*

So, the knowledge of the tunneling density of states allows the determination of tunneling current at arbitrary temperature. If $T = 0$ and the density of states of the lead is constant, $\nu_a(\omega) = \nu_0$, the tunneling density of states of the sample can be determined directly from the $I-V$-characteristic as

$$\nu_b(\omega) = 4\pi e|T_0|^2\nu_0 \left.\frac{dI}{dV}\right|_{-eV=\omega} \tag{4.23}$$

since then the Fermi function becomes a step function and the difference $n_F(\omega) - n_F(\omega+eV)$ forms a window of width eV.

4.2 Tunneling density of states in bulk superconductors

Now we want to consider a normal-superconducting tunneling junction with a normal lead and a superconducting sample. The tunneling density of states of the

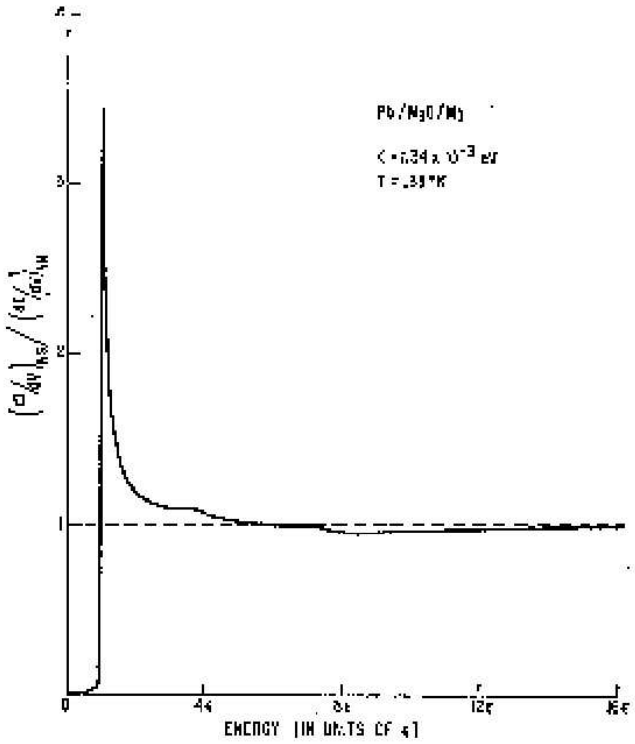

Figure 4.2: Tunneling density of states of Pb from the experiments of Giaver et. al. [21]. The gap and the singularity predicted by BCS theory (see equation (4.26)) can be seen very well.

superconductor is given by the imaginary part of the retarded Green's function (4.22). The retarded Green's function of the superconductor is (see [20])

$$G^R(\omega, \mathbf{k}) = \frac{\omega + \xi_{\mathbf{k}}}{\omega^2 - \xi_{\mathbf{k}}^2 - \Delta^2 + i0\mathrm{sign}(\omega)} \tag{4.24}$$

Thus the tunneling DoS is given by

$$\nu(\omega) = -\frac{1}{\pi}\int \frac{d^3k}{(2\pi)^3}\mathrm{Im}\, G^R(\omega, \mathbf{k}) = \nu_0 \int_{-\infty}^{\infty} d\omega\ \mathrm{sign}\,(\omega)(\omega + \xi)\delta(\omega^2 - \xi^2 - \Delta^2) \tag{4.25}$$

After calculating the integral over the δ-function, we obtain

$$\nu(\omega) = \begin{cases} \nu_0 \dfrac{|\omega|}{\sqrt{\omega^2 - \Delta^2}} & \text{for } |\omega| > \Delta, \\ 0 & \text{for } |\omega| < \Delta, \end{cases} \tag{4.26}$$

where ν_0 is the non-interacting density of states. This can be written as $\pi\nu_0\partial\xi/\partial\omega$, which is exactly the BCS quasiparticle density of states, i.e. the density of states

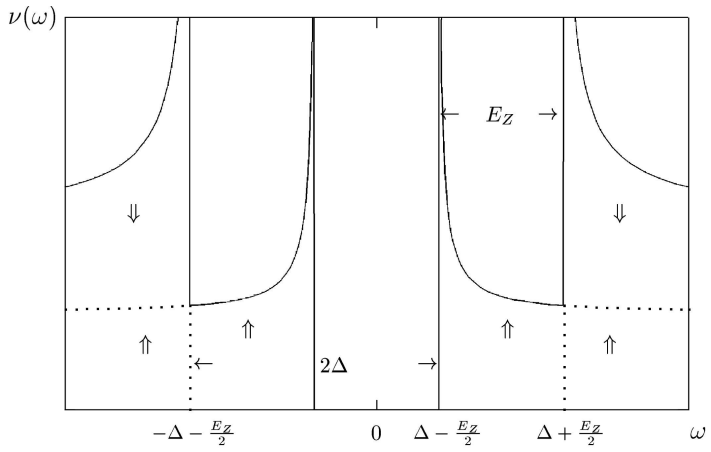

Figure 4.3: This figure from [22] shows the splitting of the tuneling DoS in bulk superconductor in magnetic field (which is small enough not to destroy the superconductivity). The singularities occur at $|\omega| = \Delta \pm E_z/2$. The Zeeman level splitting E_z corresponds to $2h$ in our notation, so $E_z/2$ is the Zeeman energy of a single spin.

of quasiparticles with the dispersion law $\omega^2 = \Delta^2 + \xi^2$. It has a gap betwen $\omega = 0$ and $\omega = \Delta$ and a singularity at $\omega = \Delta$. So tunneling experiments can serve as a check of the BCS theory. Such experiments were performed by Giaver et. al. [21] in the early sixties and provided an important confirmation of the BCS theory (see Figure 4.2).

If a magnetic field is applied, the DoS given by (4.26) splits in two diferent parts, due to the Zeeman interaction. This is shown on Figure 4.3.

4.3 Tunneling density of states above paramagnetic limit

Now we turn to the question, what happens if the grain is above paramagnetic limit, i. e. if the magnetic field is large enough to produce a transition from superconducting to a paramagnetic state as described in chapter 3. Naively one would expect that the tunneling DoS should look similar to that of a normal grain and therefore it should exhibit no singlarities. However, in experiments of Wu et. al. [8], where the tunneling DoS of disordered 2D superconducting films was measured, an anomaly above the paramagnetic limit was observed. The

tunneling DoS had a dip at the energy of the order of Zeeman energy of a single spin (see Figure 4.4).

Aleiner and Altshuler (in the following often referred to as AA) proposed a theory which explains the anomaly in the tunneling DoS above paramagnetic limit [7], [22]. We present here only the part of the theory concerning zero-dimensional systems, where no disorder averaging has to be made, as is the case for ultrasmall metallic grains.

AA explain the anomaly qualitatively in the following way [7]: " the structure of the ground state above the paramagnetic limit is similar to that without interaction ... but the spectrum of excitations changes drastically due to the interaction ... The essence of this effect is that a spin-down electron tunneling into some orbital ε_0 already occupied by a spin up electron creates an electron pair which can mix with the empty orbitals and thus interact with superconducting fluctuations. This mixing turns out to be resonant at some energy $E = E^*$ and it leads to a sharp singularity in the spectrum of one-electron excitation" (see Figure 4.5).

AA use the discrete reduced BCS model (2.1). Thus the vector index $\mathbf{k}$ in the

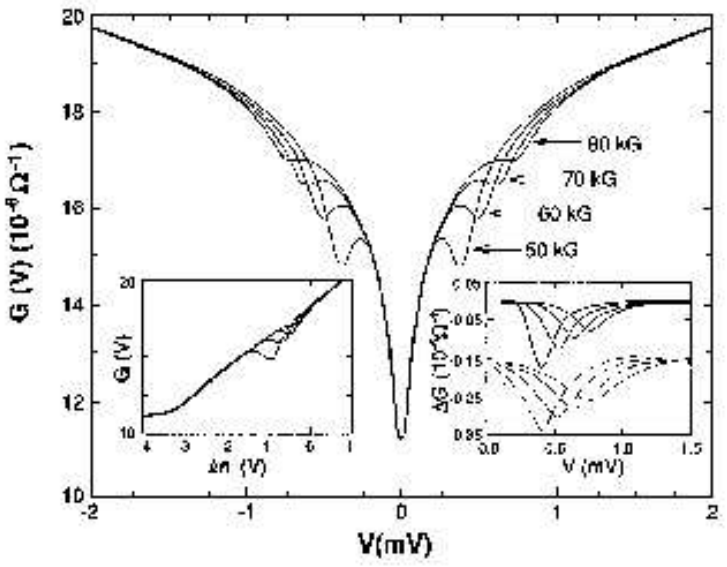

Figure 4.4: This figure from [8] shows tha experimentally measured tunnel conductance of a disordered 2D superconductoing film. The supression of the conductance at zero voltage is the usual Altshuler zero-bias anomaly. The satellite features are due to the superconducting fluctuations.

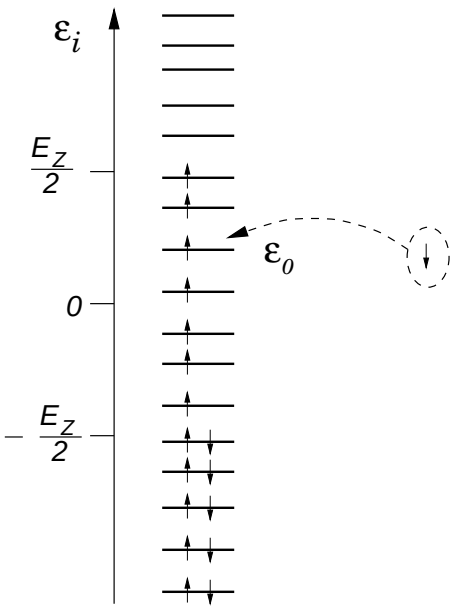

Figure 4.5: This figure is taken from [22] and shows the "structure of the superconductor above the paramagnetic limit. Electron tunneling onto the orbital ε_0 creates a spin singulet state on this orbital. At some value of ε_0 the mixing of this singlet with the empty states becomes resonant" [22].

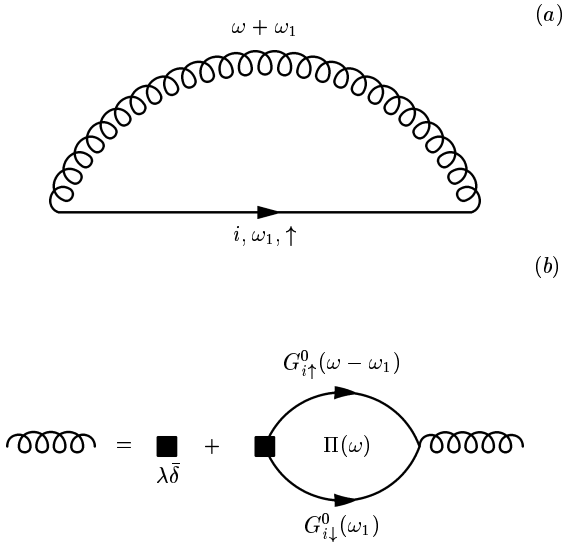

Figure 4.6: This figure from [22] shows the leading contribution to the self-energy (a) and the propagator of superconducting fluctuations (b).

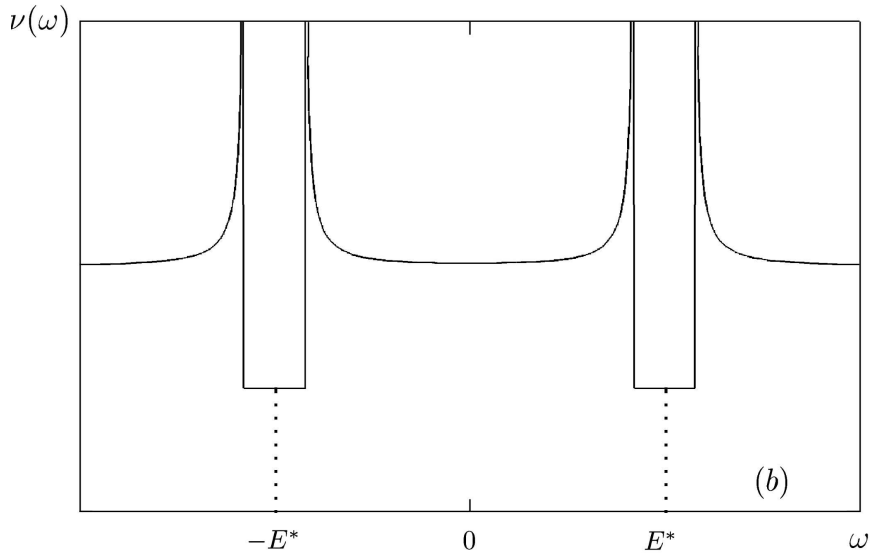

Figure 4.7: Tunneling density of states above paramagnetic limit obtained by Aleiner and Altshuler (see eq. (4.35) and text). The Figure is taken from [22].

general expression (4.22) has to be replaced by discrete index i:

$$\nu(\omega) = -\frac{1}{\pi}\sum_i \mathrm{Im}\, G^R_{i\sigma}(\omega) \tag{4.27}$$

AA calculate the single-particle retarded Green's function for the electron at the level i using the diagrammatic technique. The Dyson equation reads (since only retarded Green's functions will be used, we drop the superscript R in the following):

$$G^{-1}_{i\sigma} = G^{0\,-1}_{i\sigma} - \Sigma_{i\sigma}, \tag{4.28}$$

where $G^0_{i\sigma}$ is the non-interacting Green's function

$$G^0_{i\uparrow(\downarrow)} = (\omega_+ - \varepsilon_i \pm E_z/2)^{-1}, \tag{4.29}$$

$\omega_+ = \omega + i\,0\,\mathrm{sgn}(\omega)$ and $\Sigma_{i\sigma}$ is the self-energy.

After summing up the leading contributions to the self-energy (see Figure 4.6), AA obtain for the spin-down electron the self-energy

$$\Sigma_{i\downarrow}(\omega) = \frac{d\Delta^2}{\Omega}\frac{1}{\omega_+ + \varepsilon_i - E_z/2 + \Omega\,\mathrm{sgn}(\varepsilon_i - E_z/2)}, \tag{4.30}$$

and the Green's function

$$G_{i\downarrow}(\omega) = \frac{\omega_+ + \varepsilon_i - E_z/2 - \Omega}{(\omega_+ - \varepsilon_i - E_z/2)(\omega_+ + \varepsilon_i - E_z/2 - \Omega) - W_0^2}, \tag{4.31}$$

where

$$\Omega = \sqrt{E_z^2 - \Delta^2}, \quad W_0 = \sqrt{\frac{d\Delta^2}{\Omega}}. \tag{4.32}$$

During the calculation of the single-loop $\Pi(\omega)$ (see Figure 4.6(b)) AA replace the sum over i by an integral over $d\varepsilon_i$, thus making an approximation of a *continuous single-electron spectrum.*

Since AA consider the continuum limit, the summation over the index i in the expression (4.27) for the tunneling density of states can be replaced by an integral over $d\varepsilon_i$:

$$\begin{aligned} \sum_i G_{i\downarrow} &= \nu_0 \int_{-\infty}^{\infty} d\varepsilon_i \frac{\omega_+ + \varepsilon_i - E_z/2 - \Omega/2}{-\varepsilon_i^2 + (\omega_+ - E_z/2 - \Omega/2)^2 - W_0^2} \\ &= -i\nu_0\pi \frac{\omega - E^*}{\sqrt{(\omega - E^*)^2 - W_0^2}}, \end{aligned} \tag{4.33}$$

where

$$E^* = \frac{1}{2}(E_z + \Omega). \tag{4.34}$$

Substituting this into (4.27) AA finally find the tunneling DoS for a spin-down electron:

$$\nu_\downarrow(\omega) = \begin{cases} \nu_0 \dfrac{|\omega - E^*|}{\sqrt{(\omega - E^*)^2 - W_0^2}} & \text{for} \quad |\omega - E^*| > W_0 \\ 0 & \text{for} \quad |\omega - E^*| < W_0 \end{cases} \tag{4.35}$$

It has a gap at $|\omega - E^*| < W_0$ and singularities at $\omega = E^* \pm W_0$. For a spin-up electron the same calculations lead to expressions, which can be obtained from the corresponding expressions for the spin-down electron by changing the signs of E_z and Ω. Thus the overall density of states $\nu_\downarrow + \nu_\uparrow$ looks like in Figure 4.3. It is supressed by a factor two for $|\omega \pm E^*| < W_0$.

Chapter 5

Tunneling anomaly above paramanetic limit: new resluts

In this chapter we present the new results obtained with numerical methods (DMRG and Richardson's exact solution) for the tunneling density of states above the paramagnetic limit. The numerical methods allow us to calculate the tunneling DoS for finite N and thus to study the deviations from the continuum limit considered by Aleiner and Altshuler (see Section 4.3). The limitations of the numerical methods are the available computational power (DMRG, exact solution) and the complexity of algorithms (exact solution).

First we present the expression for the tunneling density of states, that contains the excitation energies and matrix elements. These quantities are available both with our numerical methods and with the analytical methods of Aleiner and Altshuler, so they allow us to compare analytics and numerics. In the continuum limit, which was considered by Aleiner and Altshuler, the numerical and analytical results converge, providing a useful consistency check.

The tunneling density of states of a discrete system exhibits δ-peaks, which cannot be represented graphically. Therefore we (somewhat arbitrary) replaced the δ-functions by Gaussian peaks with the width equal to the level spacing. In the continuum limit this representation yields a completely smooth density of states, since the peaks become more and more close to each other.

5.1 Tunneling DoS in terms of excitation energies and matrix elements

Expression (4.22) for the tunneling density of states contains Green's functions and therefore it can be evaluated using Feynman's diagrammatic technique. This was done by Aleiner and Altshuler [7], as described in the previous Chapter. Here we use another representation of the tunneling DoS, which can be obtained from (4.22) by expressing the imaginary part of the retarded Green's function $G^R(\mathbf{k},\omega)$ in terms of the spectral function $A(\mathbf{k},\omega)$, which in turn can be expressed in terms of eigenenergies and matrix elements of the single-particle creation operators. Namely, we use the following identities (see [23]), given in their $T=0$ form:

$$\mathrm{Im}\, G^R(\mathbf{k},\omega) = -\frac{1}{2}A(\mathbf{k},\omega), \tag{5.1}$$

$$\begin{aligned} A(\mathbf{k},\omega) = {} & \theta(\omega)\sum_n \left|\langle\psi_n^{N+1}\,|\,c_{\mathbf{k}}^\dagger|\,\psi_0\rangle\right|^2 2\pi\delta(\varepsilon_n^{N+1}-\omega) \\ & + \theta(-\omega)\sum_n \left|\langle\psi_n^{N-1}\,|\,c_{\mathbf{k}}|\,\psi_0\rangle\right|^2 2\pi\delta(\varepsilon_n^{N-1}-\omega), \end{aligned} \tag{5.2}$$

$$\text{with}\quad \varepsilon_n^{N\pm1} \equiv E_n^{N\pm1} - E_0, \tag{5.3}$$

where $|\,\psi_0\rangle$ is the ground state and E_0 it's energy for the N-particle system and $|\,\psi_n^{N\pm1}\rangle$ and $E_n^{N\pm1}$ are the eigenstates and eigenenergies of the $(N\pm1)$-particle system enumerated by a discrete index n, respectively and $\theta(\omega)$ is the Heavside step function. We see that the $(N-1)$-eigenstates contribute only for negative ω and the $(N+1)$-eigenstates contribute only for positive ω. Because of the particle-hole symmetry of the reduced BCS model, from now on we consider only the particle sector, i.e only $\omega>0$. Then the tunneling DoS introduced in Section 4.1 reads

$$\begin{aligned} \nu(\omega) \overset{(4.22)}{=} & -\frac{1}{\pi}\sum_{\mathbf{k}} \mathrm{Im}\, G^R(\mathbf{k},\omega) = \frac{1}{2\pi}\sum_{\mathbf{k}} A(\mathbf{k},\omega) \\ = & \sum_{\mathbf{k}}\sum_n \left|\langle\psi_n^{N+1}\,|c_{\mathbf{k}}^\dagger|\,\psi_0\rangle\right|^2 \delta(\varepsilon_n^{N+1}-\omega) \end{aligned} \tag{5.4}$$

The ground state of an ultrasmall metallic grain above the paramagnetic limit was discussed in Chapter 3 and has the form shown in Figure 5.1(a). It has a certain number of blocked levels immediately above and below the Fermi energy occupied by single electrons with spin parallel to the magnetic field. The remaining unblocked levels have a certain probability to be doubly occupied or empty. For $\lambda=0$ the N_F unblocked levels above ε_F are empty and N_F unblocked levels below ε_F are doubly occupied. For $\lambda\neq0$, pairing fluctuations will lead to a very

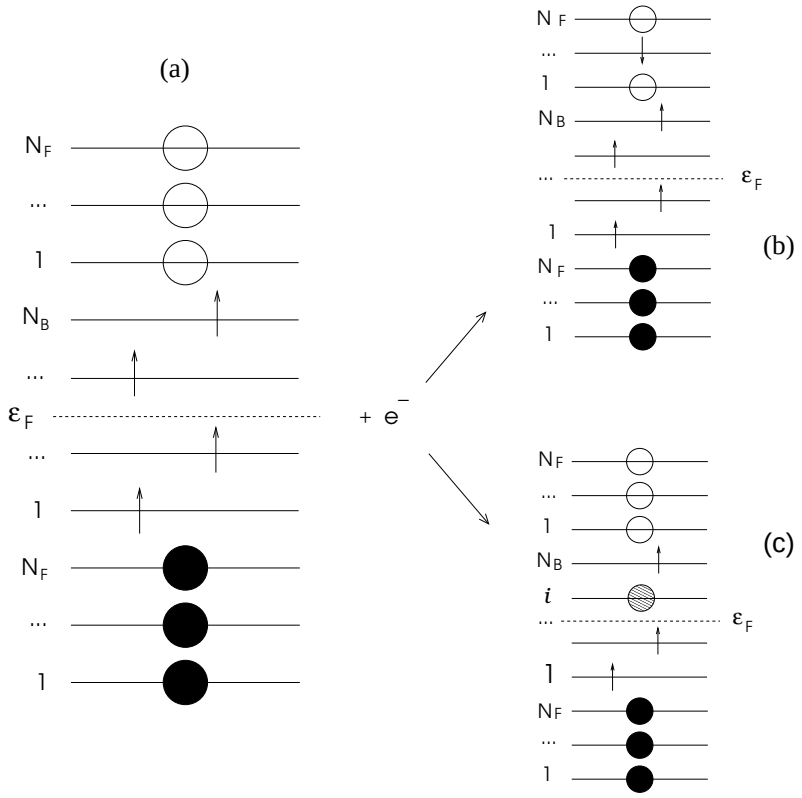

Figure 5.1: State change after the tunneling event. Adding a spin-down electron to the ground state (a) produces two different kinds of states: the new electron can block one of the previously unblocked levels (b), or it can unblock a previously blocked level i by building a pair with a single spin-up electron on it (c).

small amplitude for the highest-lying doubly occupied levels to be empty and the lowest-lying empty levels to be doubly-occupied.

Now consider what happens during a tunneling event. If the number of electrons on the grain before tunneling was N, then after the tunneling event, where an additional electron jumps onto the grain, the number of electrons becomes $N+1$. The equation (5.4) tells us that in order to obtain the tunneling density of states, we have in principle to consider all possible eigenstate of the $(N+1)$-electron grain in magnetic field. Following the general discussion of the eigenstates of the reduced BCS Hamiltonian in 2.2 and concentrating only on the ground state and the lowest-lying excitations, we consider two possibilities to obtain the $(N+1)$-eigestate from the N-ground state (see Figure 5.1):

1. blocking one of the empty unblocked level by putting the new electron on

it (Figure 5.1(b))

2. unblocking one of the N_B blocked levels by adding a spin down electron to, say, level i, thereby building a pair (shaded in Figure 5.1(c)) with the single spin-up electron already on it.)

In contrast to the situation in absence of a magnetic field, above the paramagnetic limit the first mechamnism produces a homogeneous density of states and shows no interesting features (essentially because the initially empty levels lie so far above the paired levels, and consequently are so weakly affected by pairing fluctuations, that blocking one formerly empty level has virtually no effect on pairing correlations). That is why Aleiner and Altshuler considered only the second mechanism, which we also do from now on.

Unblocking the previously singly occupied level i produces a number of possible states that can be labelled according to the distribution of filled and unfilled levels at $\lambda = 0$. We denote such states by $|\,\alpha,\, i\rangle$ and their energies by $\varepsilon_{\alpha,\,i}$, where $\alpha = 0, \ldots, \alpha_{max}$ counts all the possible states corresponding to the same new unblocked level i, in ascending order of energy. In Figure 5.2, the states $|\,0,\, i\rangle$ and $|\,1,\, i\rangle$ are shown. If we denote the ground state before tunneling by $|\,\mathrm{gs}\rangle$,

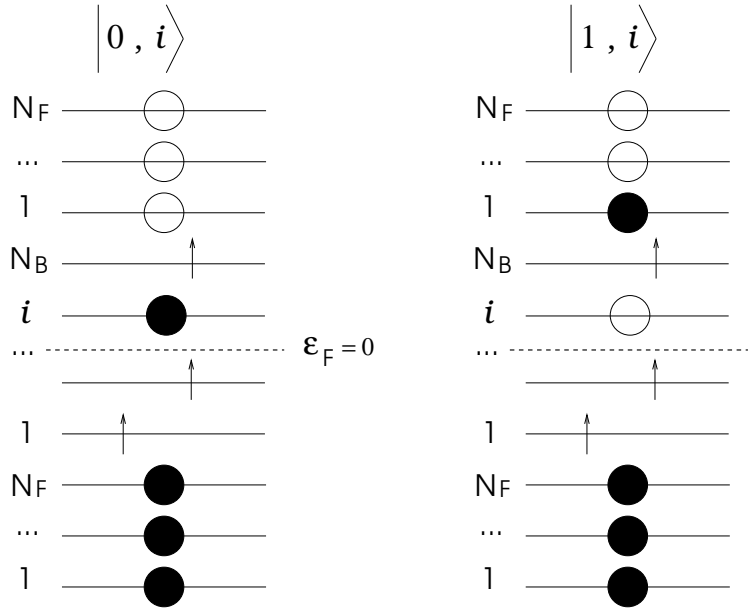

Figure 5.2: The two lowest states $|\,0,\, i\rangle$ and $|\,1,\, i\rangle$ corresponding to the new unblocked level i.

then the tunneling density of states (5.4) reads

$$\nu(\omega) = \sum_j \sum_{\alpha,i} \left| \langle \alpha,\, i \,|\, c^\dagger_{j-} \,|\, \mathrm{gs} \rangle \right|^2 \delta(\varepsilon_{\alpha,i} - \omega), \tag{5.5}$$

where we use the discrete index j to enumerate the single-particle states of the grain instead of vector index $\mathbf{k}$ in the general expression (5.4).

It is easy to see, that the matrix elements in (5.5) are non-zero only for $j = i$. Indeed, the state $|\, \alpha,\, i \rangle$ for $i \neq j$ has a single spin-up electron at level j and the state $c^\dagger_j |\, \mathrm{gs} \rangle$ has a pair of a spin-up and a spin-down electrons at level j, so that their scalar product gives zero because of the Pauli principle. So, (5.5) becomes

$$\nu(\omega) = \sum_{\alpha,i} \left| \langle \alpha,\, i \,|\, c^\dagger_{i-} \,|\, \mathrm{gs} \rangle \right|^2 \delta(\varepsilon_{\alpha,i} - \omega). \tag{5.6}$$

This means that to calculate the tunneling DoS we have to know the matrix elements $\left| \langle \alpha,\, i \,|\, c^\dagger_{i-} \,|\, \mathrm{gs} \rangle \right|$ and the excitation energies $\varepsilon_{\alpha,i}$. The DMRG method (see Section 2.4 and Appendix B) enables us to calculate only the ground state and its energy in the subspace spanned by the unblocked levels. The ground state in the subspace of the unblocked levels is the state $|\, 0,\, i \rangle$, for which, at $\lambda = 0$, the lowest unblocked levels are filled with pairs and the all higher-lying unblocked levels are empty (see Figure 5.2). So, the matrix element $\langle 0,\, i \,|\, c^\dagger_{i-} \,|\, \mathrm{gs} \rangle$ and the excitation energy $\varepsilon_{0,i}$ are available via DMRG.

The higher states $|\, \alpha > 0,\, i \rangle$ are not available with our DMRG code. Therefore we used the Richardson's exact solution to calculate the enegies $\varepsilon_{\alpha,i}$ for $\alpha > 0$ and to check the DMRG calculations for $\alpha = 0$. The matrix elements cannot be calculated with the exact solution with the available amount of computational power. But fortunately, there is a sum rule which yields an upper bound for the contribution of the higher states. Namely, if we consider all eigenstates $|\, \psi^{N+1}_n \rangle$ of the $(N+1)$-electron system, then the sum

$$S_i = \sum_n \left| \langle \psi^{N+1}_n \,|\, c^\dagger_{i-} \,|\, \mathrm{gs} \rangle \right|^2 \tag{5.7}$$

can be written as

$$S_i = \sum_n \langle \mathrm{gs} \,|\, c_{i-} \,|\, \psi^{N+1}_n \rangle \cdot \langle \psi^{N+1}_n \,|\, c^\dagger_{i-} |\, \mathrm{gs} \rangle. \tag{5.8}$$

The states $|\, \psi^{N+1}_n \rangle$ build a basis of the $(N+1)$-particle Hilbert space, so the sum $\sum_n |\, \psi^{N+1}_n \rangle \cdot \langle \psi^{N+1}_n \,|$ is equal to the identity operator. Thus we get

$$S_i = \langle \mathrm{gs} \,|\, c_{i-} c^\dagger_{i-} \,|\, \mathrm{gs} \rangle = 1 \tag{5.9}$$

Since the states $|\,\alpha,\, i\rangle$ build a subset of the states $|\,\psi_n^{N+1}\rangle$, the inequality

$$\sum_{\alpha>0} \left|\langle \alpha,\, i\,|\, c_{i-}^{\dagger}\,|\,\mathrm{gs}\rangle\right|^2 \leq 1 - \left|\langle 0,\, i\,|\, c_{i-}^{\dagger}\,|\,\mathrm{gs}\rangle\right|^2 \tag{5.10}$$

has to be be fulfilled.

5.2 Poles of the Green's function

Let us consider the retarded Green's function for the spin-down electron at the formerly singly occupied level i with energy ε_i obtained by Aleiner and Altshuler (see chapter 4.3):

$$G_{i\downarrow}^{R}(\omega) = \frac{\omega_+ + \varepsilon_i - E_z/2 - \Omega}{(\omega_+ - \varepsilon_i - E_z/2)(\omega_+ + \varepsilon_i - E_z/2 - \Omega) - W_0^2}, \tag{5.11}$$

with

$$\omega_+ = \omega + i\eta, \quad W_0 = \sqrt{\frac{d\Delta^2}{\Omega}}, \quad \Omega \equiv \sqrt{E_z^2 - \Delta^2}, \tag{5.12}$$

where $\eta = 0\,\mathrm{sgn}(\omega)$, ε_i ranges between $E_z/2$ and $E_z/2$, and $E_z/2$ gives the Zeeman energy of a single spin.

The poles of the Green's function of the N-particle system in the limit $N \to \infty$, which was considered by AA, determine the *quasiparticle excitation energies* of the system [24]. To obtain them, we have to solve the following quadratic equation for ω:

$$\omega^2 - \omega(E_z + \Omega) + E_z^2/4 - \varepsilon_i^2 + \Omega(\varepsilon_i + E_z/2) - W_0^2 = 0. \tag{5.13}$$

The solution of (5.13) reads

$$\omega_{0\,(1),\,i} = \frac{1}{2}\,(E_z + \Omega \mp \sqrt{(2\varepsilon_i - \Omega)^2 + 4W_0^2}), \tag{5.14}$$

where "$-$" and "$+$" corespond to $\omega_{0,\,i}$ and $\omega_{1,\,i}$, respectively. There are two branches in the excitation spectrum separated by $2W_0$ (see Figure 5.3). The curves $\omega_{0,\,i}(\varepsilon_i)$ and $\omega_{1,\,i}(\varepsilon_i)$ are hyperbolas symmetric with respect to the point $\varepsilon_i = \Omega/2$, $\omega = E^*$, where

$$E^* = \frac{1}{2}(E_z + \Omega) \tag{5.15}$$

After performing the partial fraction expansion of the Green's function (5.11), going into the limit $\eta \to 0$ and using the identity

$$\lim_{\eta \to 0} \frac{\eta}{x^2 + \eta^2} = \pi\,\delta(x), \tag{5.16}$$

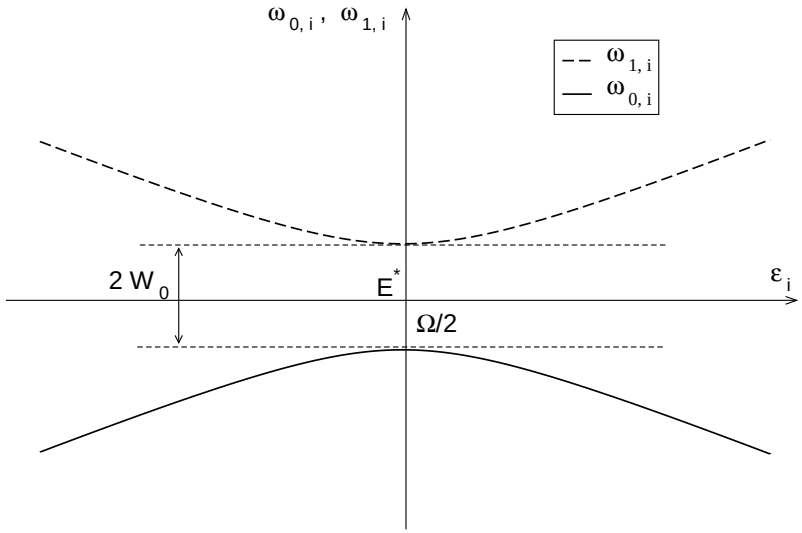

Figure 5.3: Poles of the Green's function (5.11) ω_0, ω_1 vs. energy of the additional unblocked level ε_i obtained from the Green's function (5.11). There are two branches separated by a gap W_0. The extrema points of the excitation energies lie at $\varepsilon_i = \Omega/2$.

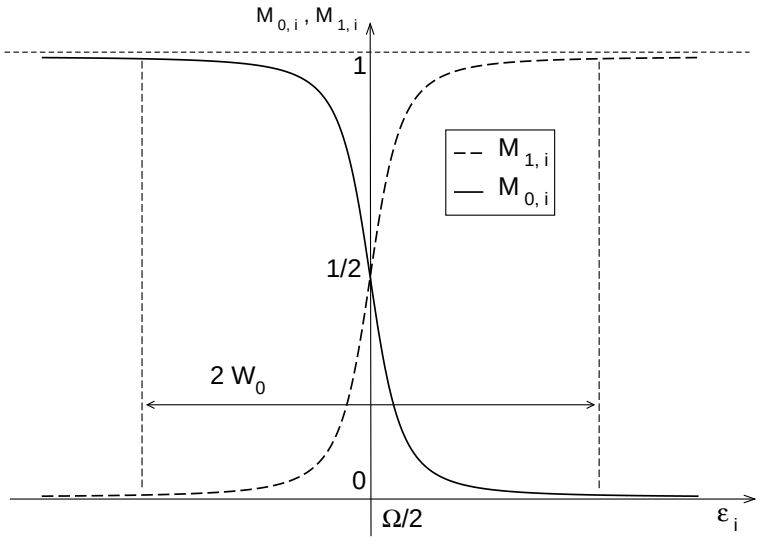

Figure 5.4: Weights $M_{0,i}$, $M_{1,i}$ of the delta peaks coresponding to the poles of the Green's function (5.11) ω_0, ω_1 vs. energy of the additional unblocked level ε_i obtained from the Green's function (5.11). The range of values of ε_i where the weights significantly change lies around the extrema points of the poles as function of ε_i (see Figure 5.3) and has the width W_0.

we get

$$\mathrm{Im}\, G_{i\downarrow} = -\pi \left(M_{0,i}\, \delta(\omega - \omega_{0,i}) + M_{1,i}\, \delta(\omega - \omega_{1,i}) \right), \tag{5.17}$$

where

$$M_{0\,(1),i} = \frac{1}{2} \left(1 \pm \frac{2\varepsilon_i - \Omega}{\sqrt{(2\varepsilon_i - \Omega)^2 + 4W_0^2}} \right), \tag{5.18}$$

where "+" corresponds to $M_{0,i}$ and "−" corresponds to $M_{1,i}$. The tunnelling DoS

$$\nu(\omega) = -\frac{1}{\pi} \sum_i \mathrm{Im}\, G_{i\downarrow} \tag{5.19}$$

thus will be the sum over delta peaks at quasiparticle energies $\omega_{0,i}$ and $\omega_{1,i}$ with the weights $M_{0,i}$ and $M_{0,i}$, respectively.

The representation (5.19) allows us to elucidate the reasons for the occurance of singularities in the tunneling DoS, which are not clear from the formal calulation of Aleiner and Alrshuler (see Section 4.3). Namely, we will see that the *singularities* occur because of the *extrema* in the quasiparticle dispersion law $\omega_{0(1),i}(\varepsilon_i)$.

The behaviour of $M_{0,i}$ and $M_{1,i}$ as functions of ε_i is shown in Figure 5.4. In the limit $d \to 0$, $W_0 \to 0$ and the matrix elements become sharp step functions around the extremum point of the excitation energies $\varepsilon_i = \Omega/2$. This means, for $d \to 0$ the weights $M_{0,i}$ will produce a cut off for the poles at $\omega_{0,i}$ for $\varepsilon_i > \Omega/2$ and the weights $M_{1,i}$ will cut off the poles $\omega_{1,i}$ for $\varepsilon_i < \Omega/2$. Looking at Figure 5.3, we see that for $d \to 0$, the sum over $\omega_{0,i}$ in (5.19) will produce δ-peaks at the energies up to $E^* - W_0$, while the sum over $\omega_{1,i}$ will produce δ-peaks at the energies from $E^* + W_0$. The tunneling DoS thus will have a gap of width $2W_0$. Since the weights of the peaks are equal, the tunneling DoS is only determined by the density of the peaks on the energy scale, which can be obtained as the derivative of the inverse functions of $\omega_{0(1),i}(\varepsilon_i)$

$$\nu(\omega) = \left. \frac{\partial \varepsilon_i}{\partial \omega_{0\,(1),i}} \right|_{\omega_{0\,(1),i} = \omega}. \tag{5.20}$$

The functions $\varepsilon_i(\omega_{0(1),i})$ can be obtained from the equation (5.13) by interpreting it as quadratic equation for ε_i, which will in general have two different roots, one of which will not contribute because of the cut off produced by the weights $M_{0,i}$ and $M_{1,i}$. Qualitatively, one readily sees from Figure 5.3, that at the edges of the gap two singularities appear since the functions $\omega_{0(1),i}(\varepsilon_i)$ have extrema at $\varepsilon_i = \Omega/2$. Performing the calculations one obtains in this way the same density of states as given by equation (4.35).

Now the following question arises: how do the quasi-particle poles $\omega_{0,i}$, $\omega_{1,i}$ and their weights $M_{0,i}$ and $M_{1,i}$ correspond to the excitation energies and matrix

elements in (5.2)? To clarify this question, we have to take the continuum limit in the finite N-expression for $\mathrm{Im}\, G_i$:

$$\mathrm{Im}\, G_i(\omega) = -\pi \sum_{\alpha} \left| \langle \alpha,\, i \,|\, c_{i-}^{\dagger} \,|\, \mathrm{gs} \rangle \right|^2 \, \delta(\varepsilon_{\alpha,\,i} - \omega) \tag{5.21}$$

In the continuum limit the energies $\varepsilon_{\alpha,\,i}$ coalesce and build continuous range of values with exception of some possible discrete points $n = 1, \ldots, n_{max}$[1]. For the continuous range the sum over the discrete index α in (5.21) becomes an integral over a continuous variable ε, whereas for discrete points the sum has to be retained. If we denote $\left| \langle \alpha,\, i \,|\, c_{i-}^{\dagger} \,|\, \mathrm{gs} \rangle \right|^2$ for the continuous range as $m(\varepsilon)$ and for the discrete points as m_n, we get:

$$\begin{aligned} -\frac{1}{\pi} \lim_{N \to \infty} \mathrm{Im}\, G_i(\omega) &= \sum_n m_n \delta(\varepsilon_n) + \int_B d\varepsilon\, D(\varepsilon)\, m(\varepsilon)\, \delta(\varepsilon - \omega) \\ &= \sum_n m_n \delta(\varepsilon_n) + m(\omega) D(\omega), \end{aligned} \tag{5.22}$$

where B denotes the continuous range of values ε and $D(\varepsilon)$ denotes the density of states at ε. The sum rule (5.10) requires

$$\sum_n m_n + \int_B d\omega\, D(\omega) m(\omega) = 1. \tag{5.23}$$

Equation (5.22) shows that continuous ranges of energy values produce no peaks and only contribute whith a smooth background. Therefore we have to identify $\omega_{0,\,i}$ and $\omega_{1,\,i}$ with some of the excitation energies $\varepsilon_{\alpha,\,i}$, which in the continuum limit are spearated from the others so that they build discrete points in the excitation spectrum for given i.

It is easy to see that the state $|\, 0,\, i \rangle$ (Figure 5.2) is energetically separated from the state $|\, \alpha,\, i \rangle$ with $\alpha > 0$, Since $|\, 0,\, i \rangle$ is the lowest state associated with tunneling into level i, in the continuum limit the equations

$$\omega_{0,\,i} = \varepsilon_{0,\,i}, \quad M_{0,\,i} = \left| \langle 0,\, i \,|\, c_{i-}^{\dagger} \,|\, \mathrm{gs} \rangle \right|^2 \tag{5.24}$$

must hold.

Comparing $\omega_{1,\,i}$ and $\varepsilon_{1,\,i}$ for $\lambda = 0$, we see that state $|\, 1,\, i \rangle$ can be one of the states that in the continuum limit correspond to the second quasiparticle pole, $\omega_{1,\,i}$. Indeed, for $\lambda = 0$ the state $|\, 1,\, i \rangle$ has at the level $N_B + 1$ above ε_F a pair of electrons, one of these is the additional electron with kinetic energy $(N_B + 1/2)\, d$

[1] This discussion follows [25], § 8.

(the first level above $\varepsilon_F = 0$ has by definition the energy $1/2\,d$) and magnetic energy h, and the other is the electron that initially was at level i in the state $|\,\mathrm{gs}\rangle$. So,

$$\begin{aligned} \varepsilon_{1,i}(\lambda = 0) &= (N_B/2 + 1/2)\,d + h + (N_B/2 + 1/2)\,d - \varepsilon_i \\ &= (N_B + 1)\,d + h - \varepsilon_i. \end{aligned} \tag{5.25}$$

For $\omega_{1,i}$ at $\lambda = 0$ we have from (5.14)

$$\omega_{1,i}(\lambda = 0) = \frac{3}{2}E_z - \varepsilon_i. \tag{5.26}$$

Now, h corresponds to $1/2E_z$ and $N_B d$ to E_z, so (5.25) becomes

$$\varepsilon_{1,i}(\lambda = 0) = \frac{3}{2}E_z - \varepsilon_i + d, \tag{5.27}$$

which differs from (5.26) only by d, which in continuum limit goes to zero.

The calculation of $\varepsilon_{1,i}$ at $\lambda \neq 0$ with the exact solution in the next section shows, that in continuum limit $\varepsilon_{1,i}$ and $\omega_{1,i}$ converge.

5.3 Tunneling DoS for finite N

Here we present our new resluts for the tunneling DoS of ultrasmall superconducting grains above paramagnetic limit. Using DMRG and exact solution, we calculated the excitation energies $\varepsilon_{\alpha,i}$, corresponding to the final states $|\,\alpha,\, i\rangle$ with $\alpha = 0,\, 1,\, 2,\, 3$ and the matrix elements $\left|\langle \alpha,\, 0\,|\, c^\dagger_{i-}\,|\,\mathrm{gs}\rangle\right|^2$, which enter the expression (5.6) for the tunneling density of states.

With DMRG we only could calculate energies $\varepsilon_{0,i}$ and the matrix elements $\left|\langle 0,\, i\,|\, c^\dagger_{i-}\,|\,\mathrm{gs}\rangle\right|^2$, since the state $|\,0,\, i\rangle$ is the ground state in the subspace spanned by unblocked levels and our DMRG code does not allow the calculation of excited states. With the exact solution we could calculate the excitation energies $\varepsilon_{o,i}$ for a large range of the values of parameters (e. g. for $\lambda = 0.4$ for N up to 300), which provided a good check of the DMRG, and the enrgies $\varepsilon_{\alpha,i}$ with $\alpha > 0$ only for a limited range of parameter values. The reason for this was mentioned in Section 2.3: the calculation of the excited states (i. e. excited states in the subspace of unblocked levels) with the exact solution requires a more complicated algorithm for the numerical solving of the Richardson's equations than the one that we used. With our algorithm the solution for the excited states is only possible for

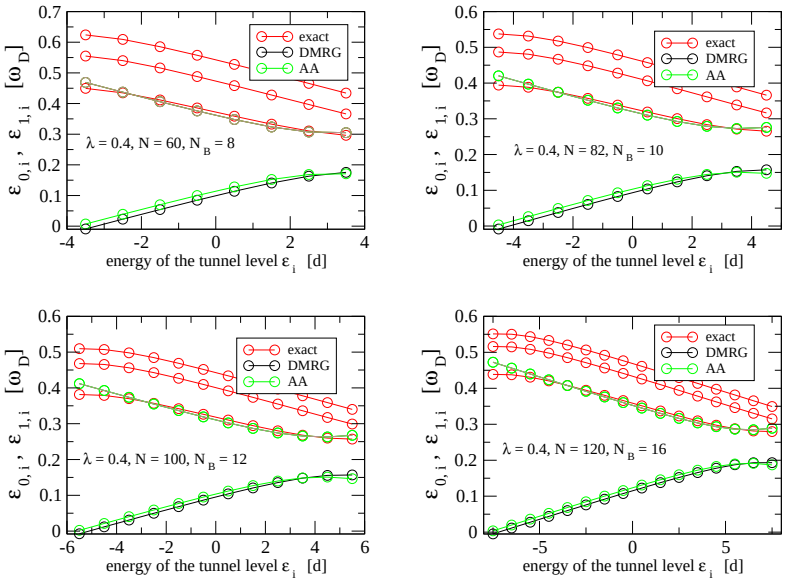

Figure 5.5: Excitation energies $\varepsilon_{0,i}$ (calculated with DMRG) and $\varepsilon_{\alpha,i}$ for $\alpha = 1, 2, 3$ (calculated with the exact solution) corresponding to tunnelling into level i and positions of the AA quasiparticle poles $\omega_{0,i}$, $\omega_{1,i}$ (see eq. 5.14) in units of ω_D vs. energy ε_i of the tunnel i ($\varepsilon_i = 0$ corresponds to the Fermi energy).

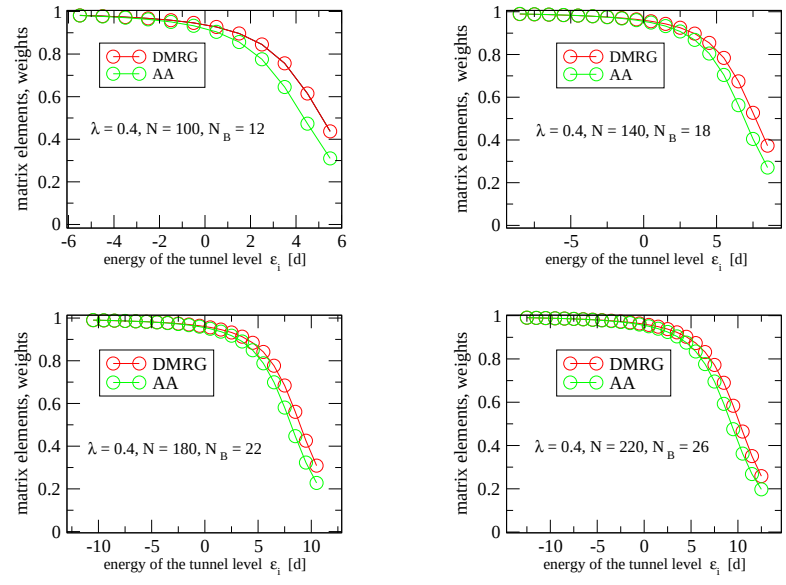

Figure 5.6: Weights of the lower AA quasiparticle peaks $M_{0,i}$ (see eq. (5.18)) and squared absolute values of the matrix elements $\left|\langle 0,\, i \,|\, c_{i-}^{\dagger} \,|\, \mathrm{gs}\rangle\right|^2$ (calculated with DMRG) for the lowest-lying excitations corresponding to tunneling into level i vs. energy of the tunnel level ε_i ($\varepsilon_i = 0$ corresponds to the Fermi energy).

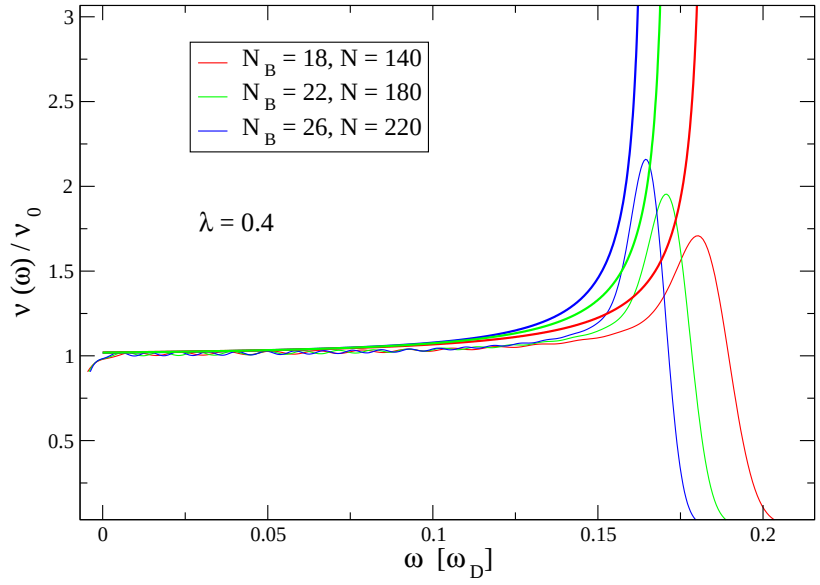

Figure 5.7: Gauss-smeared density of states $\nu(\omega)$ normalized to the non-interacting density of states ν_0 for the lowest-lying excitations $|0, i\rangle$. The thick lines are the analytical curves (see eq. (4.35)) having a singularity at $\omega = E^* - W_0$. The energy is given in units of ω_D.

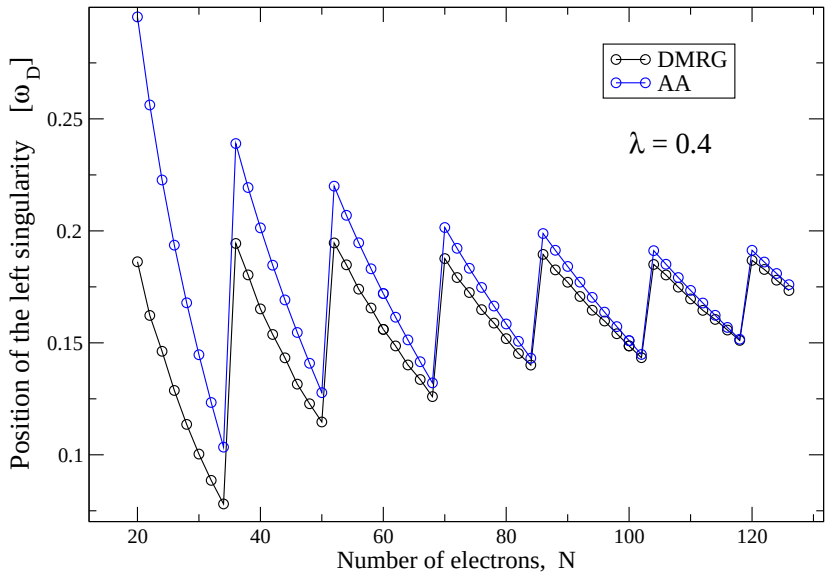

Figure 5.8: Position of the peak in the gauss-smeared numerical DoS (calculated with DMRG) for the lowest-lying excitations and position of the left singularity in the analytical DoS of AA, $E^* - W_0$, (see eq. (4.35)) in units of ω_D vs. number of electrons on the grain N.

a limited range of parameters. For example, for $\lambda = 0.4$ it was not possible to obtain a solution for $N > 120$.

In Figures 5.5 the positions of quasiparticle poles $\omega_{0,i}$, $\omega 1$, i and the excitation energies $\varepsilon_{\alpha,i}$ for $\alpha = 0,\ 1,\ 2,\ 3$ and in Figure 5.6 the weights $M_{0,i}$ and the matrix elements $\left|\langle 0,\ i \,|\, c^{\dagger}_{i-} \,|\, \mathrm{gs}\rangle\right|^2$ ate plotted as functions of the energy of the tunnel level ε_i. The number of blocked levels N_B is chosen to lie closely above the value which corresponds to the paramagnetic transition point. The coupling parameter λ has been fixed to the value $\lambda = 0.4$. The total number of electrons is varied from 60 to 120 in Figure 5.5 and from 100 to 220 in Figure 5.6. The energies are plotted in units of ω_D. We see that with increasing N, $\varepsilon_{0,i}$ and $\varepsilon_{1,i}$ converge to $\omega_{0,i}$ and $\omega_{1,i}$, respectively and $\left|\langle 0,\ i \,|\, c^{\dagger}_{i-} \,|\, \mathrm{gs}\rangle\right|^2$ converge to $M_{0,i}$.

From the excitation energies and the matrix ellements we calculated the contribution of the lowest lying excitations $|\, 0,\ i\rangle$ to tunneling density of states. We replaced the δ-functions in (5.6) by normilized gauss distribution functions:

$$\nu(\omega) = \sum_i \left|\langle 0,\ i \,|\, c^{\dagger}_{i-} \,|\, \mathrm{gs}\rangle\right|^2 \varphi(\varepsilon_{0,i} - \omega), \tag{5.28}$$

where

$$\varphi(x) = \frac{1}{\sigma\sqrt{2\pi}} \exp\left(-\frac{x^2}{2\sigma^2}\right) \quad \text{with} \quad \sigma = d/2. \tag{5.29}$$

So we smoothed the singular δ peaks and obtained the tunneling DoS as a continuous function. In Figure 5.7 the gauss-smeared tunneling density of states normalized to the non-interacting value $\nu_0 = 1/d$ is shown for $\lambda = 0.4$, $N = 100,\ 140,\ 180,\ 220$ and N_B lying closely above their values at the paramagnetic transition point.

The tunneling DoS has a peak at the values of energy closed to the maximal possible energy. It comes from the extremum point of the excitation energy $\varepsilon_{0,i}$ as function of the energy ε_i of the tunnel level i (see Figure 5.5), which leads to a high density of peaks $\varphi(\varepsilon_{0,i} - \omega)$ at the extremal value of $\varepsilon_{0,i}$. For increasing N, the peak becomes stronger, approaching the analytical singularity.

In Figure 5.8 the position of the peak in the gauss-smeared finite-N tunneling DoS and the position of the lower singularity of the analytical DoS, $E^* - W_0$, (see eq. 4.35) are plotted against N for $\lambda = 0.4$, N_B closely above the paramagnetic transition point and N changing from 20 to 130. The numerical peak always comes at lower energies than the analytical singularity. With increasing N, the numerical finite-N and analytical continuum limit curves approach each other.

What about the higher excitations ? Looking at Figure 5.5 we readily see that

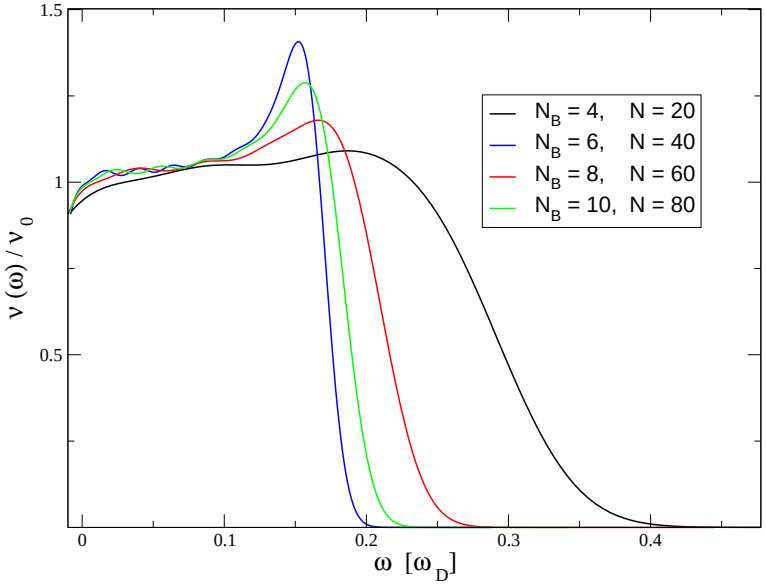

Figure 5.9: Gauss-smeared finite-N tunneling DoS due to excitations $|\,0,\,i\rangle$ for small values of N and $\lambda = 0.4$. With decreasing N, the peak vanishes.

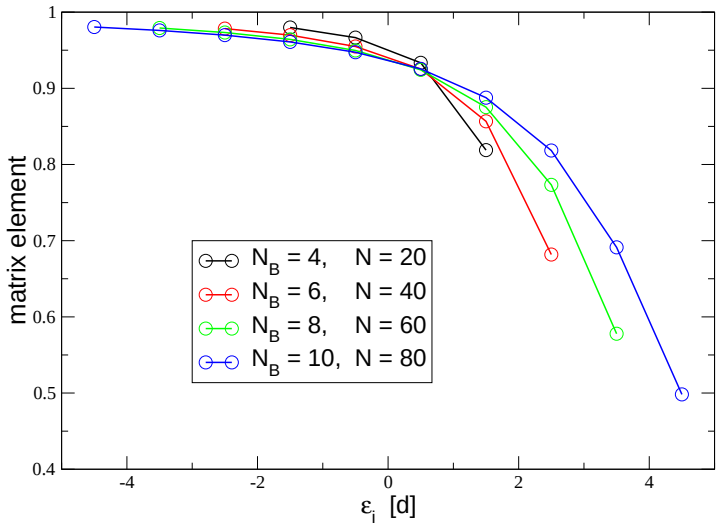

Figure 5.10: Matrix elements $\left|\langle 0,\, i\,|\, c^{\dagger}_{i\_}\,|\,\mathrm{gs}\rangle\right|^2$ for small values of N and $\lambda = 0.4$. With decreasing N, the matrix elements increase and for $N \leq 60$ become all larger than 0.5. Thus for $N \leq 60$ due to the sum rule (5.10) the contribution of the states $|\,\alpha > 0,\, i\rangle$ to the tunneling DoS is smaller than that of the lowest state $|\,0,\, i\rangle$.

there is a gap in the excitation spectrum between the states $|\,0,\,i\rangle$ and the state $|\,1,\,i\rangle$. Since we could not calculate the matrix elements for the states $|\,\alpha,\,i\rangle$ with $\alpha > 0$, we could not make plots like in Figure 5.7 for the contribution of this states to the tunneling DoS. We can only make some qualitative observations from the behaviour of the excitation energies $\varepsilon_{\alpha,\,i}$ as functions of the energy of the tunnel level ε_i and from the knowledge of the matrix elements and the sum rule (5.10).

As already mentioned, non-trivial behaviour of the tunneling density of states comes from the non-trivial behaviour of the excitation energies. A peak in the DoS at some point can only occur if the excitation energies agglomerate at this point. This happens if the the function $\varepsilon_{\alpha,\,i}(\varepsilon_i)$ has an extremum. From Figure 5.5 we see that the $\varepsilon_{\alpha,\,i}(\varepsilon_i)$ for $\alpha > 1$ only have extrema for the lowest values of ε_i while $\varepsilon_{1,\,i}(\varepsilon_i)$ also has an extrema closely below the highest value of ε_i. The sum rule tells us that the contribution of the higher states altogether and the lowest state $|\,0,\,i\rangle$ is smaller than 1.

From Figure 5.6 we see that for low levels i the lowest excitations get almost the whole weight and with increasing ε_i more weight comes up to the higher excitations. This means that the peaks corresponding to the extrema of $\varepsilon_{\alpha,\,i}(\varepsilon_i)$ for $\alpha > 1$ that lie at low ε_i have only a very low weight while the peak corresponding to the extremum of $\varepsilon_{1,\,i}(\varepsilon_i)$ which lies at a high value of ε_i could have a weight comparable to that of the lowest peak. Since we have seen that the energies $\varepsilon_{1,\,i}$ and $\omega_{1,\,i}$ converge in the large N-limit, the state $|\,1,\,i\rangle$ must be one of the states that in continuum limit contributes to the higher AA singularity at $E^* + W_0$.

So far we have seen that in the limit of large electron numbers our numerical results and the analytical results converge. We found that the state $|\,0,\,i\rangle$ is the only state that contributes to the lower singularity at $\omega = E^* - W_0$, and that the state $|\,1,\,i\rangle$ contributes to the higher singuarity at $\omega = E^* + W_0$. For the states states $|\,\alpha,\,i\rangle$ with $\alpha > 1$ we observed no singuarities. But since the energies $\varepsilon_{\alpha,\,i}$ with $\alpha > 0$ were only available for a limited range of parameters (for $\lambda = 0.4$ only N up to 120 were available), we cannot exclude the possibility that for higher values of N some of the states $|\,\alpha,\,i\rangle$ with $\alpha > 1$ also produce peaks and in the limit $N \to \infty$ contribute to the higher AA singularity.

We would like now to discuss the deviations between the tunneling DoS for small N and the continuum DoS of Aleiner and Altshuler. Instead of two singularities (for $\omega > 0$) that ocuur in the continuum limit, for small N (and generally, for finite N) there are peaks which become weaker with decreasing N as one can see from Figure 5.7. From 5.8 we see that the lowest peak in the finite-N DoS lies always lower than the lowest AA singlarity and the that distance between them

increases with decreasing N.

In Figure 5.9 the gauss-smeared tunneling DoS for small values of N and $\lambda = 0.4$ and in Figure 5.10 the corresponding matrix elements $\left|\langle 0,\, i \,|\, c_{i-}^{\dagger} \,|\, \mathrm{gs}\rangle\right|^2$ are shown. For $N = 80$ ($\Delta/d = 6.6$) there is a sharp peak, while for $N = 20$ ($\Delta/d = 1.6$) the peak has almost vanished.

The matrix elements for the lowest excitations, $\left|\langle 0,\, i \,|\, c_{i-}^{\dagger} \,|\, \mathrm{gs}\rangle\right|^2$, increase with decreasing N (see Figure 5.10). For $N \leq 60$ the matrix elements are larger than 0.5 for every i. The sume rule (5.10) then yields that the matrix elements corresponding to higher excitations must be smaller than 0.5. This means that for $N \leq 60$ the *strength of the higher peak* is *smaller* then the strength of the lower peak.

It is also interesting to see, how the peak in the DoS changes for a given grain if the magnetic field is increased. As we know from Chapter 3, above paramagnetic limit the number of blocked levels, N_B, increases linearly with the magnetic field. In Figure 5.11 we plotted the gauss-smeared finite-N tunneling DoS for $\lambda = 0.4$, $N = 100$ and different values of N_B. The strength of the peak decreases with increasing N_B. The physical reason for this is that with increasing N_B the amount of unblocked levels and thus the number of correlated electrons decreases.

In Figure 5.12 we plotted the position of the lower analytical singuarity, $E^* - W_0$, and the position of the peak in the finite-N DoS vs. N_B for the same values of λ and N as in Figure 5.11. For N_B at the paramagnetic transition point both curves almost coincide. If N_B increases, the deviation increases slightly, but remains small.

We see that in contrast to the form of the anomaly in the tunneling DoS, which in the continuum limit remains to be a singularity with increasing magnetic field, but for finite N is a peak, which strength decreases, the dependence of the position of the anomaly on the magnetic field remains for finite N almost the same as in the limit $N \to \infty$.

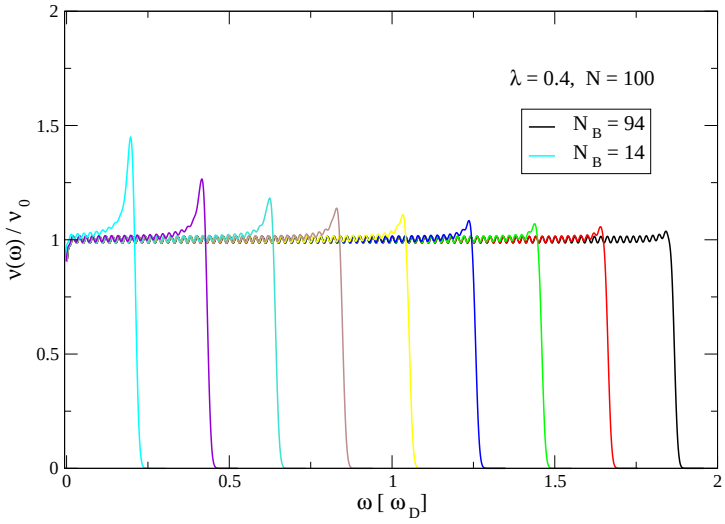

Figure 5.11: Gauss-smeared finite-N tuneling DoS for fixed λ and N and variable N_B invreasing in steps by 10 from $N_B = 14$ (leftmost step), lying closely above the paramagnetic transition point, up to $N_B = 94$ (rightmost step). The strength of the peak decreases with increasing N_B.

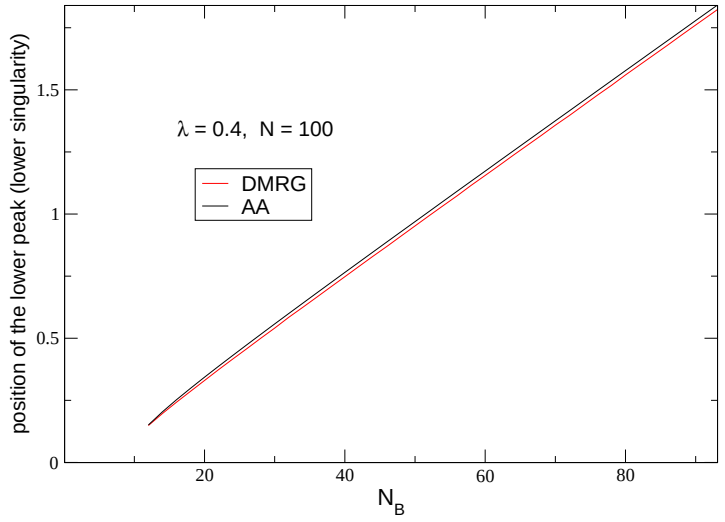

Figure 5.12: Position of the lowest peak in the finite-N DoS and the position of the lower analytical singularity, $E^* - W_0$ (see eq. (4.35)), vs. N_B for fixed λ and N .

Chapter 6

Conclusions

In this thesis we considered ultrasmall superconducting metallic grains driven by an applied magnetic field to a paramagnetic state. We analized the transition to a paramagnetic state and the tunneling density of states above the paramagnetic limit.

In Chapter 3 we considered the transition from superconducting to a paramagnetic state using DMRG and Richardson's exact solution. We calculated the magnetization as function of magnetic field by determining the energetically optimal number of the blocked (singly occupied) levels. For grains with small electron numbers N or small coupling constants λ, for which $\Delta/d \lesssim 1$, we observed that they behave purely paramagnetically: their spin increases in steps of 1 (in units of h) at uniformely spaced discrete values of magnetic field $h = d/2,\ d(1/2+1),\ d(1/2+2), \ldots$. With increasing λ or N, the spin change at the first step, S_{first}, and the corresponding magnetic field h_{first} increased (see Figures 3.5 and 3.6). We saw that for fixed λ and increasing N, S_{first} and h_{first} converged to their bulk values S_c and h_c predicted by the BCS theory (Figure 3.7).

In Chapter 5 we calculated the tunneling density of states above the paramagnetic limit for finite N numerically. This allowed to study the deviations from the theory of Aleiner and Altshuler (AA) (summarized in Section 4.3), which uses the approximation of a continuous single-electron spectrum. In Section 5.1 we expressed the tunneling density of states in terms of excited states $|\alpha, i\rangle$ that are created after a spin-down electron tunnels onto the grain and builds a pair with a spin-up electron at the previously blocked levels i (see equation (5.6) and Figures 5.1, 5.2). In Section 5.2 we analized the behaviour of the AA quasiparticle poles $\omega_{0,i}$ and $\omega_{1,i}$ for a spin-down electron tunneling into level i. We saw that

singularities ocucur due to extremal behaviour of the quasiparticle excitation energies as functions of the energy ε_i of the single-particle level i.

In Section 5.3 we calculated the excitation energies $\varepsilon_{\alpha,i}$ for $\alpha = 0, 1, 2, 3$ and matrix elements $\left|\langle 0,\, i \,|\, c^\dagger_{i-} \,|\, \mathrm{gs}\rangle\right|^2$, which enter the expression (5.6) for the tunneling DoS. In the continuum limit the excitation energies $\varepsilon_{0,i}$ and $\varepsilon_{1,i}$ converged to the analytical quasiparticle poles $\omega_{0,i}$ and $\omega_{1,i}$, respectively (see Figure 5.5), and the matrix elements $\left|\langle 0,\, i \,|\, c^\dagger_{i-} \,|\, \mathrm{gs}\rangle\right|^2$ converged to the weights $M_{0,i}$ of the lowest poles $\omega_{0,i}$ (see Figure 5.6). Thus we identified the states $|\, 0,\, i\rangle$ as the only states contributing to the lower AA singularity and the states $|\, 1,\, i\rangle$ as one of (possibly several) states contributing to the higher AA sigularity in the continuum limit.

We calculated the contribution of the states $|\, 0,\, i\rangle$ to the tunneling density of states by replacing the singular delta-peaks in the expression (5.6) with normalized gaussian peaks with the width equal to the single-electron level spacing d. Thus we obtained the tunneling DoS as a continuous function. We observed that our numerically calculated DoS had a peak, which strength increased with increasing electron number N and approached the lower AA singularity (see Figure 5.7). The position of the peak and the position of the lower AA singularity converged with increasing N (see Figure 5.8).

For small N the deviations of the tunneling DoS from the continuum limit can be summarized as follows:

- for finite N the tunneling DoS has peaks instead of singularities in the conctinuum limit
- the lower peak lies always below the lower singularity (see Figure 5.8)
- the strength of the lowest peak decreases with decreasing N, for N so small that $\Delta/d \lesssim 1$ the peak vanishes (see Figure 5.9)
- for small N the strength of the higher peak (or, possibly, several higher peaks) is lower than the strength of the lower one (see Figure 5.10)

We also analized the behaviour of the tunneling DoS for a fixed grain with increasing magnetic field h. We saw that the strength of the lower peak decreases with increasing h so that for h corresponding to N_B closely below N (i.e. when almost all spins have flipped) the peak vanished (see Figure 5.11). The position of the lower peak, however, is well described by the continuum limit expression $E^* - W_0$, (see Figure 5.12).

In this thesis we could not calculate the matrix elements for the states $|\,\alpha,\, i\rangle$ with $\alpha > 0$ and the energies of this states were only available for a limited range of parameter values (for $\lambda = 0.4$ only for N up to 120). Thus we could only estimate the contribution of these states to the anomaly by means of the sum rule (5.10). We observed that the excitation enrgies $\varepsilon_{1,\,i}$ behave extremally and thus should produce a peak in the tunneling DoS. For the energies $\varepsilon_{\alpha,\,i}$ with $\alpha > 1$ we observed no extremal behaviour. It would be interesting to investigate the contribution of the states $|\,\alpha > 0,\, i\rangle$ in more detail. An open question is, whether for large values of N the states $|\,\alpha,\, i\rangle$ with $\alpha > 1$ also produce peaks and in the limit $N \to \infty$ contribute to the higher singurarity.

Appendix A

Transformation of Richardson's equations

As we know from 2.3, the roots of the Richardson's equations (A.1) bulid pairs whose elements approach each other as the coupling parameter λ is increased.

$$1 - \sum_{j}^{U} \frac{g}{2\varepsilon_j - E_\nu} + \sum_{\mu=1(\neq\nu)}^{n} \frac{2g}{E_\mu - E_\nu} = 0, \quad \nu = 1, \ldots, n \tag{A.1}$$

After the roots become equal they turn to a complex conjugated pair. This means that the Richardson's equations become singular for some values of λ. For the sake of numerical solving of the equations this singularities must be separated by some appropriate parametrization of the Richardson's parameters E_μ.

Let n be the number of electron pairs. If we enumerate the roots from the bottom to the top, then for the ground state the pairing of the roots is as follows:

- if n is even, the roots E_{2a-1} and E_{2a}, $a = 1, \ldots, n/2$, build a pair
- if n is odd, the lowest root E_0 stays real and the roots E_{2a-1} and E_{2a}, $a = 1, \ldots, (n-1)/2$, build a pair.

Therefore we parametrize the Richardson's parameters as follows [9]:

$$\begin{aligned} E_{2a-1} &= \xi_a - i\eta_a \\ E_{2a} &= \xi_a + i\eta_a \end{aligned} \tag{A.2}$$

Here ξ is purely real, whereas η is purely imaginary before the roots become complex and real after the roots become complex. After substituting (A.2) into

the Richardson's equations, adding and substracting the equations for $\nu = 2a-1$ and $\nu = 2a$ one finds:

$$\begin{aligned}
&\frac{1}{\lambda d} - \sum_{j\neq 2a,2a-1}^{U} \frac{2\varepsilon_j - \xi_a}{(2\varepsilon_j - \xi_a)^2 + y_a(x_a^2 - \rho_a^2)} - \frac{2x_a(1+y_a)}{\rho_a^2(1-y_a)^2 - x_a^2(1+y_a)^2} \\
&+ \frac{2(E_0 - \xi_a)}{(E_0-\xi_a)^2 + \eta_a^2} + \sum_{b\neq a}^{\frac{n}{2}(\frac{n-1}{2})} \frac{4\xi_{ba}(\xi_{ba}^2 + \eta_b^2 + \eta_a^2)}{(\xi_{ba}^2 + \eta_b^2 + \eta_a^2) - 4\eta_b^2\eta_a^2} = 0, \\
&\frac{1-y_a^2}{\rho_a^2(1-y_a)^2 - x_a^2(1+y_a)^2} + \sum_{j\neq 2a.2a-1} \frac{y_a}{(2\varepsilon_j - \xi_a)^2 + \eta_a^2} \\
&- \frac{2y_a}{(E_0-\xi_a)^2 + \eta_a^2} - \sum_{b\neq a} \frac{4y_a(\xi_{ba}^2 - \eta_b^2 + \eta_a^2)}{(\xi_{ba}^2 + \eta_b^2 + \eta_a^2)^2 - 4\eta_b^2\eta_a^2} = 0,
\end{aligned} \tag{A.3}$$

where we introduced further real variables

$$\begin{aligned}
x_a &= \xi_a - \varepsilon_{2a-1} - \varepsilon_{2a}, \qquad & y_a &= \frac{\eta_a^2}{x_a^2 - \rho_a^2}, \\
\rho_a &= \varepsilon_{2a} - \varepsilon_{2a-1}, & \xi_{ba} &= \xi_b - \xi_a
\end{aligned} \tag{A.4}$$

The upper limit in the sum over b is $n/2$ if n is even and $(n-1)/2$ if n is odd. The terms containing E_0 occur only for odd n.

The equations (A.3) contain no singularities any more and can be solved for the variables x_a and y_a using the Broyden's algorithm for the initial values coppesponding to the ground state. However, for large particle numbers or large λ's the algorithm fails to converge. If the initial values corresponding to some excited state are chosen, then for λ beyond some critical value no solution with real x_a and y_a exists. The reason is that the pairing between the roots changes so that the parametrization (A.2) is not appropriate any more. It turns out that the roots behave in quite a complicated manner and the pairing can change as λ increases [15].

Appendix B

Details of the DMRG method

Sierra and Dukelsky [26] use the momentum-space DMRG algorithm to find the ground state of the reduced BCS Hamiltonian H_{BCS}. They choose the system block of the Hilbert space to be spanned by the single-electron levels above the Fermi energy ε_F and the environment block to be spanned by the levels below ε_F (see Figure B.1).

Sierra and Dukelsky exploit the particle-hole symmetry of the Hamiltonian, which means that after performing the following canonical transformation

$$c_{j\sigma} = \begin{cases} b^\dagger_{N/2+1-j,\,\sigma} & j = 1, \ldots, N/2, \\ a_{j-N/2,\,\sigma} & j = N/2+1, \ldots, N \end{cases} \tag{B.1}$$

and choosing the zero of the energy scale at $1/2\,(N+1-\lambda)$, i. e. making the transformation

$$\varepsilon_j \to \varepsilon_j - \frac{d}{2}\,(N+1-\lambda), \tag{B.2}$$

the Hamiltonian (2.1) can be rewritten in terms of $a_{j,\sigma}$, $b_{j,\sigma}$ as

$$\frac{1}{d}\,H_{BCS} = K^A + K^B - \lambda\,(A^\dagger A + B^\dagger B + AB + A^\dagger B^\dagger) - \left(\frac{N}{2}\right)^2, \tag{B.3}$$

$$K^A = \sum_{j=1,\,\sigma=\pm}^{N/2} \tilde{\varepsilon}_j\, a^\dagger_{j,\sigma} a_{j,\sigma}, \qquad A^\dagger = \sum_{i=1}^{N/2} a^\dagger_{i,+} a^\dagger_{i,-}, \tag{B.4}$$

where $\tilde{\varepsilon} = j - 1/2 + \lambda/2$ and K^B and B can be obtained from K^A and A by the particle-hole transformation $a_{i,\sigma} \leftrightarrow b_{i,-\sigma}$, under which the Hamiltonian (B.3) is invariant.

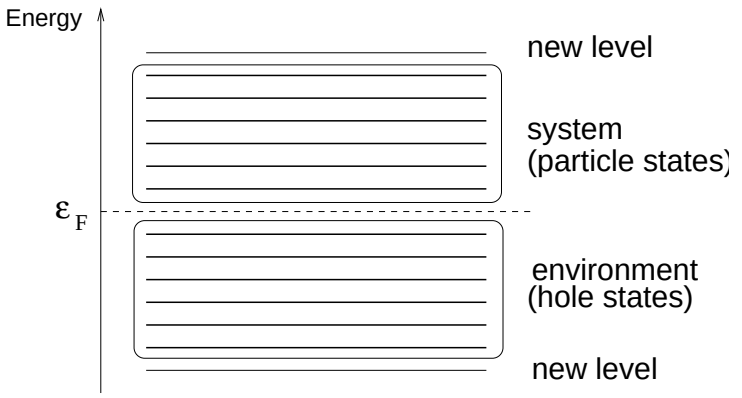

Figure B.1: Block configuration for the DMRG algorithm for the ground state of the reduced BCS Hamiltonian. The states above ε_F are the particle states, the states below ε_F are the hole states. The ground state can be written as a sum of the tensor products of particle and hole states (see equation (B.5)), which allows one to apply the infinite system algorithm.

Because of the blocking effect, only the unblocked levels have to be included into the Hilbert space, thus the basis states will have only doubly occupied or empty levels. Sierra and Dukelsky [17] introduce the paticle and hole states, the *particle states* defined as states having some *particles* (pairs of electrons with opposite spins) at some levels above Fermi surface and the other levels empty, and the *hole states* defined as the states obtained from the Fermi sea (where all levels below ε_F are occupied with pairs of electrons with opposite spins) by annihilating the electron pairs at some of the levels below ε_F and thus creating *holes* at this levels.

In terms of the particle and hole states the ground state of H_{BCS} can be represented in the form

$$|\,\mathrm{gs}\rangle = \sum_{l} \sum_{\alpha,\,\beta=1}^{m_l} \psi_{\alpha,\,\beta}(l)\,|\,\alpha, l\rangle_A \otimes |\,\beta, l\rangle_B, \tag{B.5}$$

where the particle state $|\,\alpha, l\rangle_A$ contains l particles and the hole state $|\,\beta, l\rangle_B$ contains l holes and m_l gives the multiplicity of this states. The number of particles and the number of holes have to be equal in order to conserve the particle number.

The particle states belong to the subspace of the Hilbert space spanned by the single-particle states above the Fermi surface and thus to the system block, whereas the hole states belong to the subspace spanned by the single-particle states below the Fermi surface and thus to the environment block.

In the DMRG algorithm of Sierra and Dukelsky at the beginning the superblock is chosen having $N = 4$ energy levels, being the closest two particle and hole states near ε_F. The superblock has to be diagonalized in the sector of the Hilbert space, where the number of particles is equal to the number of holes. A new superblock is builded by adding the closest particle state to the system block and the closest hole state to the environment block.

Sierra and Dukelsky exploited the particle-hole symmetry of the ground state which implies that the reduced density matrix in the particle subspace coincides with the reduced density matrix in the hole subspace. In this thesis we do not suppose the particle-hole symmetry of the states but nevertheless, we use the particle and hole states as bases of the system block and the environment block, respectively.

We used the DMRG for calculating the ground state of an ultrasmall metallic grain in presence of a magnetic field in Chapter 3 and for calculating the excited states $|\,\alpha,\,0\rangle$ and matrix elements $\langle 0,\,i\,|\,c^{\dagger}_{i-}\,|\,\mathrm{gs}\rangle$ entering the tunneling density of states in Chapter 5 (see equation (5.6) and Figure 5.2). The DMRG can be applied to these states since they are ground states in the Hilbert spaces spanned by the corresponding unblocked levels.

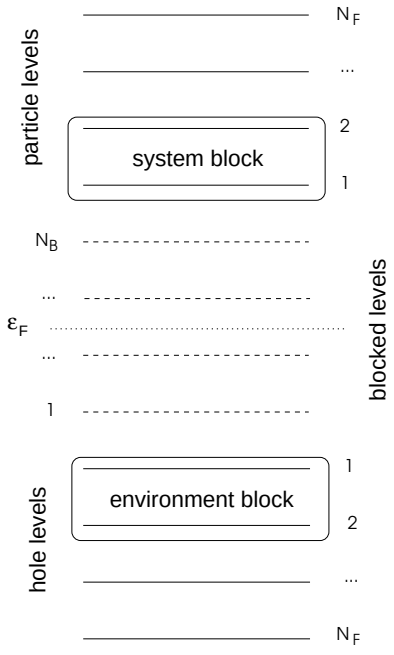

Figure B.2: Intial superblock and environment block configuration for the ground state in presence of a magnetic field.

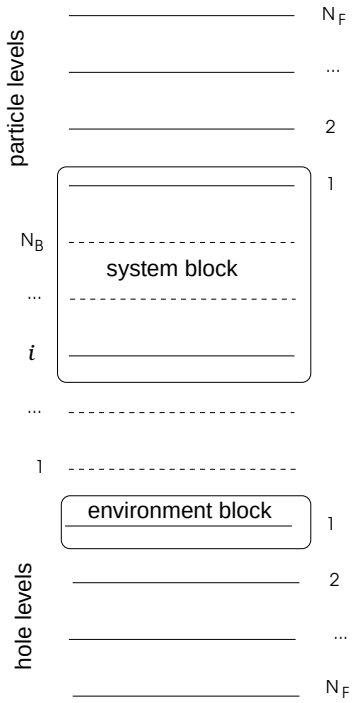

Figure B.3: Initial system block and environment block configuration for the state $|\,0,\,i\rangle$. The system block contains the additional unblocked level and the lowest particle level of the ground state. Dashed lines denote blocked levels not included into the Hilbert space of DMRG.

The ground state in presence of a magnetic field is discussed in Chapter 3.3. It has $N_B/2$ blocked levels above ε_F and $N_B/2$ blocked levels below ε_F. This levels only contribute with their kinetic energy and do not interact with the electrons at the unblocked levels. The DMRG algorithm is used to calculate the energy E_{int} of the interacting electrons for different values of N_B in order to find the energetically optimal value of N_B. The only change in the algorithm compared to the algorithm for the ground state without magnetic field is that the particle levels start at $\varepsilon_F + N_B/2\,d$ and the hole levels start at $\varepsilon_F + N_B/2\,d$ (d is the level spacing) (see Figure B.2).

For the calculation of the state $|\,0,\,i\rangle$ and the matrix elements $\langle 0,\,i\,|\,c^\dagger_{i-}\,|\,\mathrm{gs}\rangle$ we take into account that there is an additional unblocked level i, i. e. an additional particle level, and that the number of particles N_p and the number of holes N_h are now related by $N_p = N_h + 1$. For this reason the initial superblock is choosed containing the lowest hole state and the lowest two particle states (see Figure B.3). This choice insures that after subsequently adding a new particle and new

hole after some number of steps we reach all the levels.

Furthermore, in order to calculate the matrix elements between the ground state and the state $|0, i\rangle$, both states have to be represented in the same basis. This is acchieved by letting the level i be unblocked during the calculation of the ground state and assigning to it a huge energy of say $10000d$, which makes it very unprobable for this level to be occupied. The same initial superblock is chosen for the ground state as was chosen for the state $|0, i\rangle$. Then all steps of the algorithm are made simultaniously for the both states. At the step where the reduced density matrices are calculated for the ground state and the state $|0, i\rangle$, they are devided by 2 and added. The obtained matrix is diaoganalized and its m eigenstates with the highest eigenvalues provide a basis optimal for representing the both states.

Bibliography

[1] J. Bardeen, L. N. Cooper, and J. R. Schrieffer, Phys. Rev. **108**, 1175 (1958).

[2] B. L. Altshuler and P. A. Lee, Physics Today **41(12)**, 36 (1988).

[3] C. T. Black, D. C. Ralph, and M. Tinkham, Phys. Rev. Lett. **76**, 688 (1996).

[4] J. von Delft, Ann. Phys. (Leipzig) **10**, 219 (2001).

[5] F. Braun, J. von Delft, D. C. Ralph, and M. Tinkham, Phys. Rev. Lett. **79**, 921 (1997).

[6] R. Richardson, Phys. Lett. **3**, 277 (1963).

[7] I. L. Aleiner and B. L. Altshuler, Phys. Rev. Lett. **79**, 4242 (1997).

[8] W. Wu, J. Williams, and P. W. Adams, Phys. Rev. Lett. **77**, 1139 (1996).

[9] J. von Delft and D. Ralph, Physics Reports **345**, 61 (2001).

[10] K. A. Matveev, L. I. Glazman, and A. I. Larkin, Phys. Rev. Lett. **85**, 2789 (2000).

[11] M. Tinkham, *Introduction to superconductivity* (McGraw-Hill, New York, 1996).

[12] N. N. Bogoliubov, Soviet Physics JETP **34**, 58 (1958).

[13] J. G. Valatin, Nuovo Cimento **7**, 843 (1958).

[14] R. Richardson and N. Sherman, Nucl. Phys. **52**, 221 (1964).

[15] J. Dukelsky and G. Sierra, cond-mat **0207640**, (2002).

[16] S. White and R. Noack, in *Density matrix renormalization: a new numerical method in physics* (Springer, Berlin Heidelberg, 1999).

[17] J. Dukelsky and G. Sierra, Phys. Rev. B **61**, 12302 (2000).

[18] N. W. Ashcroft and N. D. Mermin, *Solid state physics* (Saunders College Publishing, New York, 1976).

[19] L. S. Levitov and A. V. Shytov, *Green's functions. Exercises with solutions (in russian)* (Physmatlit, Moscow, 2002).

[20] G. D. Mahan, *Many-particle physics* (Kluwer Academic/Plenum Publishers, New York, 2000).

[21] I. Giaver, H. R. Hart, and K. Megerle, Phys. Rev. **126**, 941 (1962).

[22] I. L. Aleiner and B. L. Altshuler, Phys. Rev. B **58**, 5757 (1998).

[23] J. W. Negele and H. Orland, *Quantum many-particle systems* (Perseus Publishing, Cambridge, Massachusetts, 1998).

[24] A. A. Abrikosov, L. P. Gorkov, and I. E. Dzyaloshinski, *Methods of quantum field theory in statistical physics* (Dover Publications, Inc., New York, 1963).

[25] L. D. Landau and E. M. Lifschitz, *Lehrbuch der theoretischen Physik, Band IX: Statistische Physik, Teil 2.* (Akademie-Verlag, Berlin, 1992).

[26] J. Dukelsky and G. Sierra, Phys. Rev. Lett. **83**, 172 (1999).

Danksagung

Mein herzlicher Dank gilt:

- Prof. Dr. Jan von Delft, der mir die Möglichkeit zur Anfertigung dieser Diplomarbeit am Lehrstuhl für theoretische Festkörperphysik gegeben hat und von dem ich vieles gelernt habe
- Dominique Gobert, der mich während der Diplomarbeit betreut hat und immer ansprechbar und hilfsbereit war
- allen Mitarbeitern des Lehrstuhls von Delft für eine angenehme und freundliche Atmosphäre und Hilfsbereitschaft
- meinen Eltern und Großeltern und meinem Bruder Sergei für ihre moralische und finanzielle Unterstützung.

Erklärung

Hiermit versichere ich, daß ich diese Diplomarbeit selbstständig und nur mit den angegebenen Quellen und Hilfsmitteln angefertigt habe.

München, den 08. August 2003

Igor Gazuz